UNIVERSITY OF TURKU

Elucidation of mechanisms underlying TGF-β-driven downregulation of HSF2 in breast cancer progression

M.Sc. Molecular Biosciences, Cell Biology
Master's thesis

Author:
Katriina Eskelinen

11.12.2025
Turku

Master's thesis

Degree program and subject: M.Sc. Molecular Biosciences, Cell Biology
Author: Katriina Eskelinen
Title: Elucidation of mechanisms underlying TGF-β-driven downregulation of HSF2 in breast cancer progression
Supervisors: M.Sc. Jannica Roininen, M.Sc. Jenny Pessa, Prof. Lea Sistonen (Åbo University)
Pages: 57 (+6 appendix) pages
Date: 11.12.2025

Abstract

Metastasis is the leading cause of cancer-related mortality, and its initiation requires cancer cells to acquire invasive traits. A central mechanism enabling this switch is epithelial-to-mesenchymal transition (EMT), a morphological program that cancer cells can hijack. Recent findings show that transforming growth factor-β (TGF-β) suppresses heat shock factor 2 (HSF2) transcription in breast cancer cells concomitantly with EMT, yet the regulatory mechanism underlying this repression remains unknown. This thesis aimed to verify that TGF-β-mediated HSF2 suppression is transcriptional, and to identify the specific *HSF2* promoter regions and transcription factors (TFs) mediating this downregulation.

To distinguish transcriptional repression from enhanced mRNA decay, HS578T human breast cancer cells were treated with the transcription inhibitor actinomycin D with or without TGF-β, followed by qRT-PCR-based mRNA stability measurements. To pinpoint the *HSF2* promoter area mediating TGF-β-induced HSF2 repression, truncated *HSF2* promoter fragments were cloned into luciferase reporters and transfected into HS578T cells, followed by luciferase reporter assays. A DNA affinity purification (DAP) protocol was established and optimized to isolate TGF-β-responsive TFs using biotinylated promoter probes incubated with nuclear extracts from ± TGF-β-treated HS578T cells, followed by streptavidin-based capture.

The results revealed that TGF-β does not promote mRNA degradation, indicating that downregulation occurs at the transcriptional level. Reporter assays identified a 0.5-kb region immediately upstream of the 5' untranslated region as the principal *HSF2* promoter segment mediating TGF-β-responsive HSF2 downregulation. The piloted DAP, however, lacked sufficient specificity for mass spectrometry, indicating that further methodological optimization is required before TF identification can proceed.

In conclusion, this thesis demonstrates that TGF-β suppresses HSF2 transcriptionally and identifies the proximal 0.5-kb promoter region as the key regulatory element mediating this repression. These findings provide a foundation for identifying the TGF-β-responsive TFs acting on the 0.5-kb promoter region and for understanding how TGF-β-driven transcriptional regulation contributes to invasive behavior during breast cancer progression.

Keywords: breast cancer, cancer invasion, cellular plasticity, epithelial-to-mesenchymal transition, heat shock factor 2, transforming growth factor-β

Table of contents

Abbreviations:

AD	Transactivation domain
Akt	Protein kinase B
AMPK	AMP-activated protein kinase
CHIP	C-terminus of Hsp70-interacting protein
DBD	DNA-binding domain
DAP	DNA affinity purification
DNMT1	DNA methyltransferase 1
ECM	Extracellular matrix
EDTA	Ethylenediaminetetraacetic acid
EMT	Epithelial-to-mesenchymal transition
EMT-TF	Epithelial-to-mesenchymal transition transcription factor
FBS	Fetal bovine serum
HEPES	4-(2-hydroxyethyl)-1-piperazineethanesulfonic acid
HIF-1/2	Hypoxia-inducible factor 1/2
HRP	Horseradish peroxidase
HSE	Heat shock element
HSF	Heat shock factor
HSR	Heat shock response
JAK/STAT	Janus kinase / signal transducer and activator of transcription
JNK	c-Jun N-terminal kinase
Luc	Luciferase reporter gene
MET	Mesenchymal-to-epithelial transition
miRNA	MicroRNA
MMP	Matrix metalloproteinase
mTOR	Mammalian target of rapamycin
NELF	Negative elongation factor
NP-40	Nonidet P-40 or igepal
ONPG	o-nitrophenyl-β-D-galactopyranoside
PBS	Phosphate-buffered saline
PCR	Polymerase chain reaction
PI3K	Phosphoinositide 3-kinase
PTM	Post-translational modification
qRT-PCR	Quantitative real-time PCR
Ras	Rat sarcoma virus oncogene family
RD	Regulatory domain
RhoA/ROCK	Ras homolog family member A / Rho-associated kinase
SBE	Smad-binding element
SDS-PAGE	Sodium dodecyl sulfate-polyacrylamide gel electrophoresis
Smad	Small mothers against decapentaplegic
Sox4	SRY-box transcription factor 4
SUMO	Small ubiquitin-like modifier
TGF-β	Transforming growth factor beta
TGF-βR1/2/3	TGF-β receptor type 1/2/3
TGF-βRAP1	TGF-β receptor-associated protein 1
TF	Transcription factor
UTR	Untranslated region
ZEB	Zinc-finger E-box binding transcription factor
ZO-1	Zonula occludens-1

1 Introduction

1.1 Epithelial-to-mesenchymal transition

Cellular plasticity refers to the ability of cells to reprogram their phenotypic and morphological identities in response to environmental cues and pleiotropic signaling (Pérez-González et al. 2023). The principal mechanism underlying cellular plasticity is epithelial-to-mesenchymal transition (EMT), during which epithelial cells lose their defining characteristics and acquire mesenchymal, fibroblast-like properties. These lost epithelial traits include cuboidal morphology, apicobasal polarity, and intercellular adhesions including tight, gap, and adherens junctions and lateral desmosomes (Brabletz et al. 2021; Dongre and Weinberg 2019). The acquired mesenchymal state is characterized by cytoskeletal reorganization, transition to spindle shaped morphology, establishment of front-rear polarity through actin cytoskeleton remodeling, and a shift in cell-matrix adhesions toward more transient and dynamic forms, all collectively increasing mobility.

The phenotypic changes are accompanied by transcriptional and translational reprogramming, particularly the downregulation of key epithelial markers involved in maintaining tissue integrity and intercellular cohesion. Among these is E-cadherin, a transmembrane protein central to adherens junctions, which mediates calcium-dependent cell-cell adhesion and is critical for the maintenance of epithelial architecture and tissue integrity (Koch et al. 1997). Claudins and occludins are integral components of tight junctions, forming selective barriers that regulate paracellular permeability and maintain cell polarity (Kuo et al. 2022). Zonula occludens-1 (ZO-1) is a cytoplasmic scaffolding protein that anchors tight junction components to the actin cytoskeleton, contributing to the stability and function of junctional complexes. The collective downregulation of epithelial markers weakens intercellular adhesions, destabilizes pre-existing junctional complexes, and impairs the formation of new cell-cell contacts. Loss of epithelial integrity facilitates cellular detachment from the epithelial sheet and enables invasive behavior – key features of EMT (Puisieux et al. 2014).

Concurrently, mesenchymal markers become upregulated, reflecting the transition toward a more motile and invasive cellular phenotype. N-cadherin facilitates more dynamic and transient cell-cell adhesions that support cellular movement (Cao et al. 2019). Vimentin, an intermediate filament protein, plays a central role in cytoskeletal reorganization, thereby enhancing cellular plasticity and motility (Satelli and Li 2011). Fibronectin, a high molecular weight glycoprotein of the extracellular matrix (ECM), provides a structural

scaffold that supports directional migration and cell adhesion (Ruoslahti 1981). Matrix metalloproteinases (MMPs) are a family of zinc-dependent endopeptidases that degrade various ECM components, enabling tissue remodeling and invasion through surrounding stroma (de Almeida et al. 2022). β-catenin, when localized to the nucleus, reflects activation of the Wnt signaling pathway – a key regulator of EMT, stemness, and proliferation (Lamouille et al. 2014; Scheel et al. 2011; Xue et al. 2024). The expression patterns of these markers are frequently assessed to characterize cellular states in *in vitro* research.

EMT is reversible, as the mesenchymal-like cells can revert to an epithelial state, a process known as mesenchymal-to-epithelial transition (MET). However, the properties of cells undergoing EMT/MET do not consistently conform to either epithelial or mesenchymal cell types. Instead, they often exhibit intermediate states with mixed characteristics from the epithelial-mesenchymal spectrum (Figure 1). Therefore, EMT and MET are more accurately characterized as dynamic continua, rather than as rigid transitions between binary cellular states. As such, researchers have also collectively referred to these processes as epithelial-mesenchymal plasticity, which more accurately describes the intermediate transitions, especially in their pathogenetic contexts (De Blander et al. 2024).

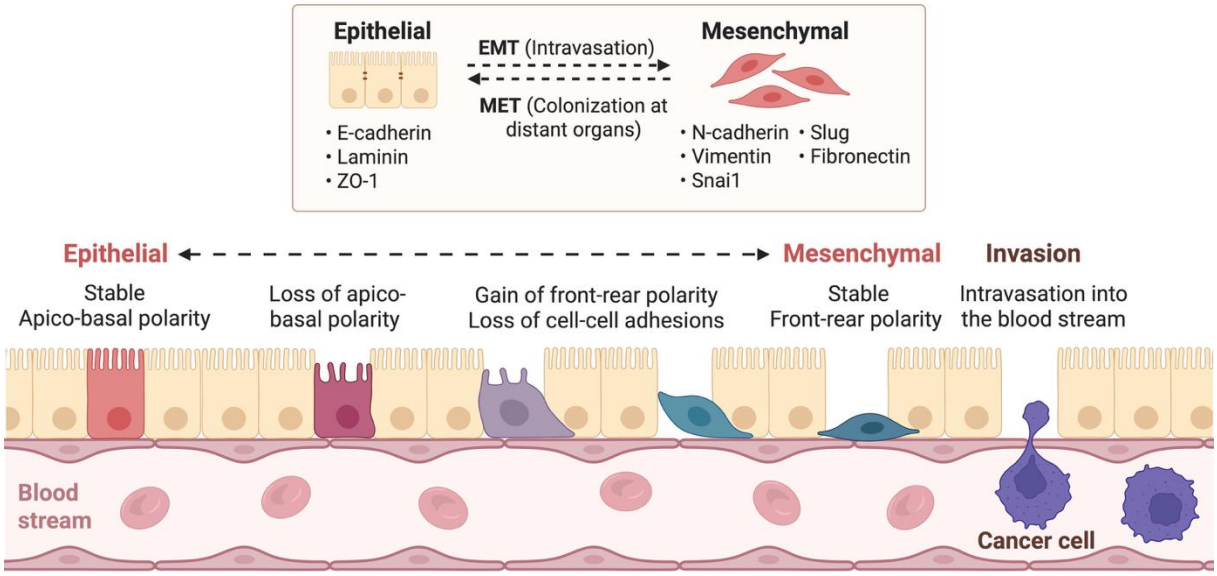

Figure 1. Epithelial-to-mesenchymal transition (EMT) process and markers of epithelial and mesenchymal states. Epithelial cells maintain apicobasal polarity and stable cell-cell contacts. During EMT, cells progressively lose their epithelial characteristics and acquire mesenchymal traits including cytoskeletal remodeling, front-rear polarity, and enhanced motility. These changes facilitate detachment from the surrounding epithelium and the underlying basal layer and the subsequent invasion into surrounding tissues, eventually enabling cancer cells to enter the bloodstream. Here, EMT is depicted as a conceptual continuum; however, *in vivo*, cells commonly occupy hybrid epithelial/mesenchymal states, and invasion can occur without completion of EMT.

1.1.1 EMT's role in physiological and pathological processes

The characteristics of cells undergoing EMT vary depending on the context in which it occurs. Therefore, EMT is categorized into three types: type I occurs during embryogenesis, type II during wound healing and fibrosis, and type III in malignant transformation (Kalluri and Weinberg 2009).

EMT was first observed in embryonic development (Greenburg and Hay 1982) and later recognized as an ancient physiological cellular program that enabled metazoans to evolve complex tissue types and organize into distinct layers (Thiery and Sleeman 2006; Yang et al. 2020). EMT facilitates many crucial processes during embryogenesis, among which are gastrulation, heart development (Sun et al. 2021) and neural crest migration, the process that gives rise to diverse tissues including peripheral nerves, craniofacial cartilage and the adrenal medulla (Nieto et al. 2016). EMT activation, however, is not solely confined to early development; it can also be induced in adults during wound healing, where EMT-derived mesenchymal cells further transition into a myofibroblast phenotype, leading to the enhanced deposition of ECM (Di Gregorio et al. 2020; Sisto and Lisi 2024). Under physiological conditions, myofibroblasts undergo apoptosis following wound healing and re-epithelialization (Di Gregorio et al. 2020). However, persistent activation by chronic inflammation prevents their clearance, resulting in excessive collagen deposition and fibrosis (Di Gregorio et al. 2020; Marconi et al. 2021; Sisto and Lisi 2024). As this fibrotic process advances, EMT-induced transformation of epithelial parenchyma into nonfunctional tissue drives progressive structural and functional decline, a phenomenon observed in organs such as the liver, kidneys, intestine, and lungs (Di Gregorio et al. 2020; Marconi et al. 2021).

Beyond developmental processes and fibrosis, EMT is also implicated in malignant transformation, with its contribution recognized as one of the hallmarks of cancer. Rather than stochastically obtaining multiple specific mutations required to transition into an invasive phenotype, pre-malignant epithelial cells can reactivate this latent plasticity program to acquire invasive and disseminative properties (Brabletz et al. 2021; Katsuno et al. 2013; Weinberg 2023). These traits are obtained through oncogenic signaling pathways that affect gene regulation through transcriptional activation, post-transcriptional mechanisms, or epigenetic changes, all of which will be discussed in detail in the next section (1.1.2). By acquiring invasive traits, motile cancer cells can intravasate into the bloodstream and subsequently extravasate into distant tissues, where they may undergo MET to revert to an

epithelial state, proliferate, and form micrometastases (Weinberg 2023). Therefore, EMT holds a key role in the invasion-metastasis cascade.

EMT does not occur in all cancer cells, as a tumor consists of a heterogenous mass of cells, most of which are epithelial. Instead, in carcinomas, which are cancers of epithelial origin, EMT may occur transiently at the tumor boundaries, giving rise to a "tumor invasive front" with the scale of EMT depending on the tumor's origin (Debnath et al. 2021; Nieto et al. 2016). For example, in breast cancer the extent of EMT is observed to be more prominent, as intravasated tumor cells circulating in the bloodstream often exhibit a more mesenchymal phenotype (Nieto et al. 2016).

In addition to promoting invasive properties, EMT-inducing transcription factors (TFs) also participate in other cellular processes that may confer survival advantages, including the inhibition of apoptosis and senescence and the enhancement of immunosuppressive mechanisms, thereby further increasing metastatic potential (Thiery and Sleeman 2006; Yang et al. 2020). Moreover, EMT imparts stem-like features to transitioned cells, granting them self-renewal capacity, tumor-initiating potential, and resistance to drugs and chemotherapeutic agents (Dongre and Weinberg 2019; Galle et al. 2020; Wendt et al. 2012). These multifaceted changes during EMT not only enable dissemination from the primary tumor but also foster the establishment of secondary growths in distant tissues.

1.1.2 Induction of EMT

As a plasticity program involving widespread changes in cellular identity, EMT induction is governed by pleiotropic signaling on all levels of gene regulation. On the transcriptional level, EMT activation involves the cooperation of several TFs, collectively referred to as EMT-TFs, that share the ability to repress genes encoding epithelial characteristics and/or promote those encoding mesenchymal properties (Giarratana et al. 2024). These include Snail, Slug and zinc-finger E-box binding (Zeb) TFs, and basic helix-loop-helix factor Twist (Huber et al. 2005; Lamouille et al. 2014). Specifically, many EMT-TFs repress E-cadherin and activate N-cadherin and MMPs. The pleiotropic activation of these TFs also leads to the upregulation of vimentin and fibronectin genes (Scheel et al. 2011). Several signaling pathways, which are modulators of both embryogenesis and tumorigenesis, co-operate to regulate the expression of these EMT-TFs, including Notch (Wang et al. 2013), hypoxia-inducible factors 1 and 2 (HIF-1/2) (Yang et al. 2024), Wnt (Xue et al. 2024), Nuclear Factor Kappa B (Mirzaei et al. 2022), and Rat sarcoma virus (Ras) (Lee et al. 2024). Additionally, the cytokine transforming growth

factor-β (TGF-β) often plays a dominant role and its involvement in EMT will be discussed later in detail (Section 1.2.4).

Epigenetics refers to the regulation of gene activity through chemical modifications that do not alter the underlying DNA sequence. The modifications influence gene expression by altering chromatin structure, thereby modulating the accessibility of DNA to the transcriptional machinery. In the context of EMT, widespread cellular reprogramming and changes in EMT marker expression are driven by such epigenetic mechanisms. Specifically, EMT-TFs recruit histone-modifying enzymes to alter promoter activity, promoting cellular plasticity and contributing to cancer progression. These histone modifications include the Snail-mediated recruitment of a histone demethylase LSD1, which removes a dimethyl group from H3K4 – a mark associated with active chromatin – at the E-cadherin promoter (Lin et al. 2010). The presence of LSD1 is essential for sustaining E-cadherin repression, as its absence leads to partial gene reactivation (Lin et al. 2010). Notably, LSD1 also participates in a broader transcriptional repressive complex alongside other chromatin modifiers at EMT-TF promoters, where it contributes to EMT-TF suppression (Choi et al. 2015). This reinforces the epigenetic silencing necessary for EMT progression and the acquisition of stem-like properties. DNA methyltransferase 1 (DNMT1) regulates EMT in a context-dependent manner, acting as both a suppressor and activator. It maintains DNA methylation during replication and silences gene expression by binding repressive histone marks at EMT-TF promoters like Zeb2 and Snail (Skrypek et al. 2017; Tan et al. 2022). While repressing these promoters inhibit EMT, DNMT1 may also promote it by hypermethylating tumor suppressor genes and activating oncogenic pathways such as Wnt/β-catenin signaling (Skrypek et al. 2017; Tan et al. 2022). In addition to EMT-TFs, microRNAs (miRNAs) involved in EMT are also tightly regulated through epigenetic mechanisms.

MiRNAs are small non-coding RNA molecules that can repress gene expression post-transcriptionally by binding to sequence-specific mRNAs to mark them for destruction or hinder ribosome access to inhibit translation (He and Hannon 2004). Since miRNAs are estimated to target 10–40% of mRNA sequences, they regulate a wide array of biological processes. When dysregulated, they can contribute to malignant transformation by promoting pathological EMT (Zaravinos 2015). The downregulation of the miR-200 family is especially important in EMT, as it represses the EMT-TFs Zeb1 and Zeb2, which are transcriptional repressors of E-cadherin (Gregory et al. 2008). This aligns with observations that invasive breast cancer cell lines, which have undergone EMT to acquire a mesenchymal phenotype,

lose their miR-200 expression (Hill et al. 2013). Moreover, forced overexpression of miR-200 has been observed to inhibit EMT and promote metastatic colonization (Korpal et al. 2011). MiRNAs also participate in shaping and responding to the tumor microenvironment, modulating cellular interactions and signaling pathways that further influence EMT and cancer progression (Guo et al. 2015).

The tumor microenvironment consists of cellular and non-cellular components that interact dynamically, forming a milieu characterized by hypoxia, acidosis, and scarcity of nutrients such as glucose, fatty acids, and amino acids (Shi et al. 2022). Many aspects of the tumor microenvironment are believed to induce EMT in the peripheral cells. Tumor-associated hypoxia promotes glycogen accumulation via the HIF-1, facilitating EMT induction, energy provision in a nutrient-restricted environment, and protection against cancer cell death (Ji et al. 2023; Shi et al. 2022). Additionally, hypoxia triggers metabolic reprogramming, shifting primary ATP production towards glycolysis (Shi et al. 2022). Glucose-6-phosphate, the first metabolic intermediate of glycolysis, is redirected to the pentose phosphate pathway, providing essential biochemical building blocks that support uncontrolled tumor growth. Moreover, glucose metabolism is redirected toward the hexosamine biosynthesis pathway, leading to abnormal glycosylation patterns that are frequently observed in cancer cells, enhancing cell adhesion, migration, and immune checkpoint modulation (Carvalho-cruz et al. 2018). Cancer cells relying on glycolysis produce significant amounts of lactate, furthering the acidification of the tumor microenvironment (Carvalho-cruz et al. 2018).

To summarize, EMT is orchestrated by EMT-TFs and epigenetic regulators, both of which are influenced by the conditions of their microenvironment. Together, these factors drive cellular plasticity and support invasive traits in cancer cells.

1.2 TGF-β

TGF-β is a member of the TGF-β superfamily, a diverse group of structurally conserved growth factors and cytokines that regulate key cellular characteristics and processes, including metabolism, morphogenesis, proliferation, apoptosis, wound healing, inflammation, and differentiation (Wendt et al. 2012). TGF-β exists in three isoforms – TGF-β1, TGF-β2, and TGF-β3 – each encoded by separate genes. Despite having distinct genetic origins, these isoforms share 60–80% sequence homology (Lichtman et al. 2016). While TGF-β1–3 exhibit distinct spatial and temporal expression patterns and may even exert antagonistic effects in certain contexts (Chan et al. 2008; Urban et al. 2023), they are often collectively referred to as

“TGF-β”. Among the three isoforms, TGF-β1 is the most prevalent and biologically significant, as it regulates immune response homeostasis and facilitates tissue repair in response to injury or inflammation (Lodyga and Hinz 2020). Given its multifaceted regulatory roles, even subtle perturbations in homeostatic TGF-β1 signaling can lead to profound consequences, contributing to tissue fibrosis and cancer, both marked by sustained chronic inflammation. Accordingly, TGF-β is tightly regulated, with minor changes in concentration capable of eliciting a wide array of biological responses (Feng et al. 2016). In this thesis, TGF-β refers to the TGF-β1 isoform.

1.2.1 The biosynthesis of TGF-β

TGF-β1–3 are synthesized as inactive precursor polypeptides, composed of the C-terminal mature cytokine, a central regulatory component, and an N-terminal signaling sequence (Derynck et al. 1985). The signaling sequence directs the polypeptide into the endoplasmic reticulum, where it is cleaved (Deng et al. 2024). The remaining polypeptide then dimerizes and translocates to the Golgi apparatus, where the regulatory component is cleaved but remains bound non-covalently to the mature cytokine as a “latent complex”, masking its receptor binding site and rendering the TGF-β inactive (Deng et al. 2024; Dubois et al. 1995). TGF-β may be stored in its inactive form in the extracellular space through binding of the latent complex to the ECM (Lichtman et al. 2016). TGF-β activation occurs through the dissociation of the latent complex from the mature TGF-β dimer, a process that can be triggered by various mechanisms. The best-characterized pathway involves integrins binding to the latent complex, inducing a conformational change that facilitates the release of active TGF-β (Annes et al. 2002). Other activation mechanisms feature proteases, such as the serum protease thrombin, interactions with proteins in the matrix or cell membrane, reactive oxygen species, and acidification, a phenomenon often observed in tumor microenvironments (Deng et al. 2024; Jullien et al. 1989; Lichtman et al. 2016; Moustakas and Heldin 2012).

Once active with the receptor-binding site exposed, TGF-β is free to bind to its receptors of which there are three subtypes: type 1 (TGF-βR1), type 2 (TGF-βR2), and type 3 (TGF-βR3, betaglycan). TGF-βR1 and TGF-βR2 are serine/threonine kinases, and together they form the heterotetrameric TGF-β receptor complex responsible for initiating TGF-β signaling. In contrast, betaglycan functions as a co-receptor that lacks intrinsic signaling capability, instead regulating the bioavailability of TGF-β by binding and presenting it to the TGF-βR2 (Bilandzic and Stenvers 2011).

1.2.2 TGF-β signaling pathways

All three isoforms, TGF-β1–3, signal through the TGF-βR2 receptor. Upon TGF-β ligand binding to TGF-βR2, TGF-βR1 is recruited and subsequently phosphorylated at its serine residues by TGF-βR2 (Deng et al. 2024; Giarratana et al. 2024; Huang and Chen 2012) (Figure 2). Once activated, TGF-βR1 phosphorylates downstream transducers, triggering intracellular signaling cascades. In the canonical pathway, the small mothers against decapentaplegic (Smad) family of proteins serve as the primary mediators. These include the receptor-regulated Smads (R-Smads), Smad2 and Smad3, phosphorylated by TGF-βR1, and the common-mediator Smad, Smad4, forming an essential complex with activated R-Smads (Hata and Chen 2016). Upon phosphorylation, Smad2 and Smad3 bind to Smad4 forming a heterotrimeric complex that translocates into the nucleus (Deng et al. 2024; Giarratana et al. 2024). Within the nucleus, Smad complexes bind Smad-binding elements (SBEs) to regulate gene expression. However, because their affinity for individual SBEs is low, robust transcriptional regulation generally requires multiple SBE repeats and cooperative interactions with DNA-binding transcription factors or co-activators (Deng et al. 2024). Many Smad-interacting cofactors contain intrinsic histone modification capabilities, enabling TGF-β signaling to modulate chromatin accessibility and impose epigenetic changes (Meng et al. 2016). Smad activity may also be regulated through post-translational modifications (PTMs) such as phosphorylation or ubiquitination, with the former influencing activation and the latter inducing proteasomal degradation (Deng et al. 2024; Huang and Chen 2012; Liu et al. 2024). Together these regulatory mechanisms fine-tune the intensity and duration of TGF-β/Smad signaling.

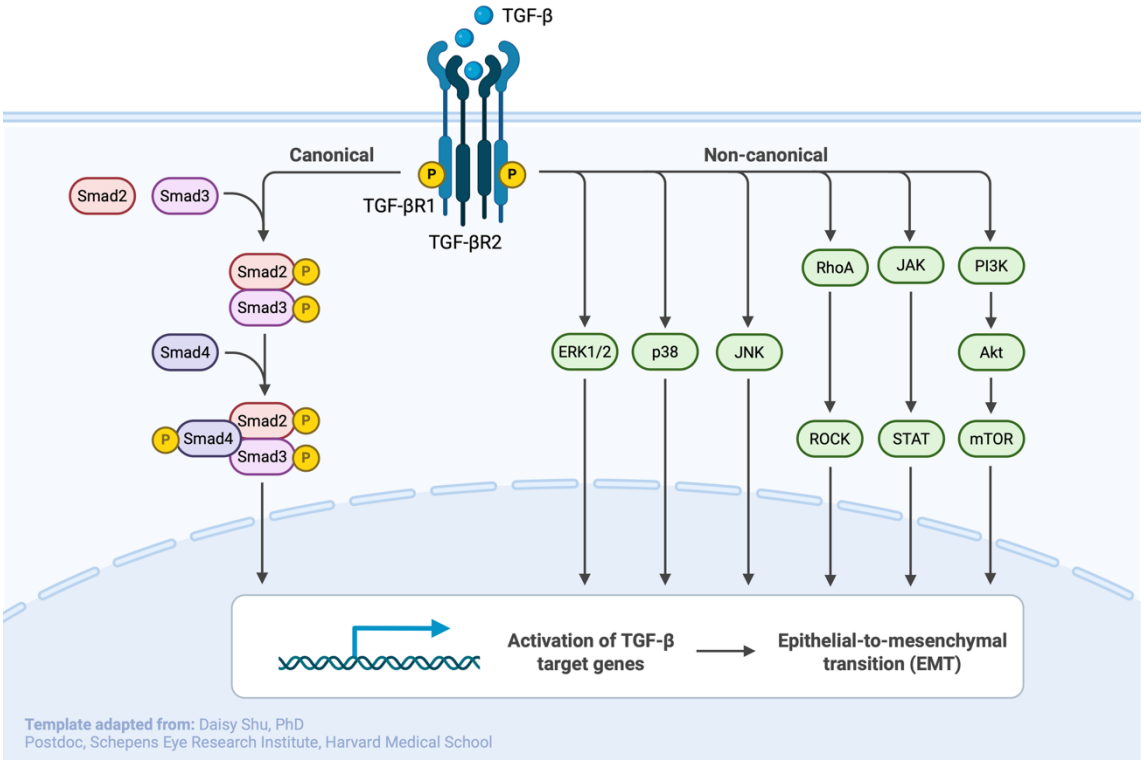

Figure 2. Canonical and non-canonical TGF-β pathways in EMT. Upon ligand binding, the TGF-β type II receptor (TGF-βR2) recruits and phosphorylates the type I receptor (TGF-βR1). Canonical signaling proceeds through receptor-regulated Smads, Smad2 and Smad3, which are phosphorylated by TGF-βR1 and subsequently form a complex with the common-mediator Smad4. This trimeric complex translocates into the nucleus to regulate transcription of TGF-β-responsive genes. Non-canonical signaling involves several pathways including Erk1/2, p38, JNK, RhoA/ROCK, JAK/STAT, and PI3K/Akt/mTOR. Collectively, these signaling pathways coordinate diverse transcriptional regulation, which may lead to epithelial-to-mesenchymal transition (EMT).

TGF-β signaling also induces the expression of inhibitory Smads, which establish negative feedback mechanisms to maintain homeostasis. For example Smad7 attenuates signaling by recruiting phosphatases to dephosphorylate TGF-βR1, which terminates downstream signaling, and by recruiting ubiquitin ligases that target TGF-βR1 for degradation, thereby reducing receptor availability for ligand binding (Deng et al. 2024; Giarratana et al. 2024). In cancer, however, this negative feedback regulation can be disrupted. TGF-βR-associated binding protein 1 (TGF-βRAP1), whose expression is itself induced by TGF-β, competes with ubiquitin ligases for access to TGF-βR1 and thus prevents receptor degradation (Liu et al. 2024). By stabilizing TGF-βR1, TGF-βRAP1 prolongs Smad phosphorylation and sustains TGF-β signaling activity. In liver cancer, this aberrant reinforcement of TGF-β signaling has been shown to promote cancer stemness and contribute to drug resistance (Liu et al. 2024).

Beyond Smad-dependent signaling, TGF-β also activates non-canonical pathways via the TGF-βR2/ TGF-βR1 receptor complex, leading to the activation of various well-known

intracellular signaling cascades such as PI3K/Akt/mTOR, Erk, p38, JNK, JAK/STAT, and RhoA/ROCK, which contribute to broader cellular responses (Bierie and Moses 2006; Giarratana et al. 2024) (Figure 2). It is important to note that canonical and non-canonical TGF-β pathways do not operate independently; instead, their interplay is required for the precise modulation of cellular responses to TGF-β stimulation (Giarratana et al. 2024).

1.2.3 TGF-β in cancer

In various cancers including breast, lung and pancreatic cancer, TGF-β is overexpressed, which is associated with disease progression, metastasis, and patient mortality (Bierie and Moses 2006; Massagué 1998). Essentially, TGF-β plays a dual role functioning as both a tumor suppressor and a tumor promoter depending on the cellular and microenvironmental contexts.

In the early stages of cancer, TGF-β suppresses tumor growth by maintaining genomic integrity, repressing mitogenic factors, inhibiting tumorigenic inflammation, and promoting cytostasis or apoptosis in pre-malignant cells (Ikushima and Miyazono 2010; Leonardo-Sousa et al. 2025). In later stages, TGF-β shifts from an anti-tumor to a tumor-promoting role, driving malignant transformation. This is driven by aberrant TGF-β signaling, mutations, losses of allelic heterozygosity in TGF-β receptors or pathway components, or epigenetic changes, resulting in impaired tumor-suppressive functions (Bierie and Moses 2006; Deng et al. 2024; Leonardo-Sousa et al. 2025; Massagué 2008; Wendt et al. 2012). A crucial aspect of tumor promotion is the co-option of inflammation-dampening signaling, which is transformed to enforce immune tolerance. This involves TGF-β inhibiting the development and proliferation of innate and adaptive immune cells, including CD^{4+} helper and CD^{8+} killer T-cells, natural killer cells, macrophages, and dendritic cells (Ikushima and Miyazono 2010). Concurrently, TGF-β stimulates the generation of regulatory T-cells that suppress T-cell activation and effector functions, hindering the recognition and elimination of malignant cells and allowing them to propagate within the tumor microenvironment (Ikushima and Miyazono 2010; Lodyga and Hinz 2020; Shen et al. 2017).

An insightful analogy can be found in normal physiology, where TGF-β maintains the quiescent hematopoietic stem cell niche in the bone marrow (Yamazaki et al. 2009). Although not oncogenic, this finding reflects TGF-β's broader capability to regulate cell survival, suppress apoptosis, and preserve stem-like states – properties that cancer cells can later exploit. Such observations raise the possibility that TGF-β may similarly support cancer stem

cell niches and contribute to early tumorigenesis. Because both physiological and malignant stem-like states rely on high cellular plasticity, EMT emerges as a major plasticity program through which TGF-β can reshape cellular phenotypes and promote tumor progression.

1.2.4 TGF-β in EMT

TGF-β signaling has been observed to induce EMT in various physiological and pathological contexts. In development, EMT is involved in the formation of the embryonic heart (Potts and Runyan 1989), the cardiac heart valves (Romano and Runyan 2000), and the regression of Müllerian ducts in male rat sex organ development (Trelstad et al. 1982). Following embryogenesis, TGF-β signaling participates in wound healing by attracting endothelial cells and fibroblasts to cutaneous injuries and by serving as a differentiation factor that promotes the formation of myofibroblasts (Lee and Massagué 2022). In cancer, TGF-β-induced EMT contributes to tumor progression and ultimately facilitates metastasis (Dongre and Weinberg 2019). Beyond altering morphology, TGF-β also reprograms the cellular phenotype to support invasion and metastasis. It reshapes the transcriptional landscape to enhance myofibroblast activation and angiogenesis, increase the expression of MMP2 and MMP9, and stimulate the deposition of ECM components such as fibronectin and collagen (Javelaud and Mauviel 2005; Meng et al. 2016; Moustakas and Heldin 2012). These alterations lead to ECM degradation and tissue reconstitution – key characteristics required for invasion.

TGF-β promotes pro-invasive effects by serving as a primary inducer of EMT through the upregulation of EMT-TF expression (Debnath et al. 2021; Lee and Massagué 2022; Thiery and Sleeman 2006; Yang et al. 2020). These include Slug, Snail, Twist and Zeb, which can be induced through both canonical and non-canonical pathways (Jalali et al. 2012; Lamouille et al. 2012; Thuault et al. 2006, 2008; Vincent et al. 2009). Specifically, the Smad3/4 complex interacts with the regulatory promoter regions of Snail, promoting its transcription. Once activated, the Smad3/4-Snail1 complex binds to promoter regions of genes encoding epithelial adhesion proteins E-cadherin and occludin, leading to their TGF-β-mediated repression (Vincent et al. 2009).

TGF-β signaling has also been observed to regulate EMT post-transcriptionally by influencing the biogenesis of miRNAs, many of which are believed to govern EMT (Guo et al. 2015; Nieto et al. 2016). For example Smad signaling downstream of TGF-β suppresses the miR-200 family through the upregulation of Zeb TFs (Bracken et al. 2008; Gregory et al. 2008; Peinado et al. 2007). Since miR-200 normally suppresses Zeb, TGF-βR1 and Smad2,

its downregulation amplifies Zeb1 and Zeb2 expression, accelerating EMT progression (Bracken et al. 2008; Moustakas and Heldin 2012; Wendt et al. 2012). TGF-β-mediated Smads may also interact with high mobility group A2, a non-histone binding chromatin factor, to enhance the binding of Smads to the E-cadherin repressor Snail1's promoter (Thuault et al. 2008).

Non-canonically, TGF-β induces EMT via activation of the Erk pathway, leading to upregulation of Ras, Raf, MEK1/2, and Erk1/2, while promoting Erk phosphorylation and enhanced kinase activity, which drive cytoskeletal remodeling, junctional disassembly, and fibroblast-like morphology (Xie et al. 2004). Furthermore, Oft and coworkers (1996) reported that TGF-β-induced EMT not only initiates fibroblastoid transformation in Ras-transformed epithelial cells but also sustains an invasive and metastatic phenotype through autocrine signaling and dynamic epithelial-stromal interactions. Since the transition to a mesenchymal morphology is a key facilitator of tumor invasion, TGF-β plays a central role in driving this process through EMT induction.

TGF-β signaling also influences cancer metabolism, further reinforcing EMT. It upregulates glucose transporter 1 in various cancers, correlating with the expression of EMT markers (Li et al. 2010; Liu et al. 2016). Additionally, this metabolic reprogramming involves the TGF-β-induced stimulation of glycolysis through the upregulation of key glycolytic enzymes. The resulting increase in glycolytic rate leads to lactate accumulation, causing acidosis within the tumor microenvironment, which further amplifies TGF-β-driven EMT (Shi et al. 2022). Thus, TGF-β signaling establishes a synergistic relationship between EMT and glucose metabolism, creating a feedback loop that promotes tumor progression and the onset of invasive properties.

Despite the growing body of work suggesting that TGF-β-driven EMT is tumor-promoting, it has also, counterintuitively, been observed to exert tumor-suppressive functions. In pancreatic cancer cells, TGF-β-induced EMT triggers Sox4 to shift from a tumor-promoting role to functioning as a driver of apoptosis, leading to the programmed cell death of malignant cells (David et al. 2016). Therefore, TGF-β-driven EMT, while predominantly associated with malignancy in cancer, should not be regarded exclusively as pro-tumorigenic.

Taken together, these findings highlight the multifaceted role of TGF-β in regulating EMT through transcriptional, post-transcriptional, and metabolic mechanisms. While often associated with tumor promotion and metastasis, TGF-β's functions are context-dependent and may include tumor suppressive effects. This complexity has prompted increasing

attention in additional regulatory pathways that interact with or modulate TGF-β-driven EMT programs. One such pathway is the cellular heat shock response (HSR), a conserved stress-adaptive mechanism that protects protein homeostasis, i.e. proteostasis. Emerging evidence suggests that stress-response pathways can influence cellular plasticity and contribute to TGF-β-induced EMT (Pessa et al. 2025). Therefore, the role of this stress response in EMT should be investigated further.

1.3 Heat shock response

Cells encounter various types of stress throughout their lifetime. To ensure survival, they have evolved protective mechanisms that safeguard the vulnerable molecular machinery essential for life, largely through stress-induced transcriptional responses. The first observations linking cellular stress to transcriptional changes were reported in 1962 by Ferruccio Ritossa, when a malfunctioning incubator altered the temperature of *Drosophila* cultures. This temperature shift produced a distinct puffing pattern in the salivary gland polytene chromosomes of *Drosophila* larvae. These oversized chromosomes are easily visualized under a microscope, where puffing patterns reflect sites of active transcription. The emergence of new puffing patterns suggested that environmental disturbance could activate transcription in a distinct manner. Notably, Ritossa's findings were initially dismissed as his manuscript was rejected by *Nature* for lacking biological significance (Capocci et al. 2014). In retrospect, however, the discovery proved profoundly important: the phenomenon Ritossa observed represents the HSR, an ancient and evolutionarily conserved cellular survival mechanism now recognized across all organisms.

The HSR is activated in response to proteotoxic stress that disrupts proteostasis (Pessa et al. 2024). Despite its name, the HSR does not protect the cell merely from elevated temperatures, but also from other stressors which disrupt proteostasis, including oxidative damage, heavy metals, and the aging-associated chronic expression of metastable aggregation-prone proteins (Morimoto 2011). However, while the HSR is fundamentally adaptive, its dysregulation can contribute to oncogenic survival pathways, linking stress tolerance to tumor progression (Dai et al. 2012). To safeguard the cell, HSR induces the transcription of molecular chaperones known as heat shock proteins (Hsps), which assist in protein folding, prevent protein aggregation, and target damaged proteins for degradation (Pessa et al. 2024). Collectively, Hsps contribute to restoring proteostasis and thereby protect cells from the accumulation of non-functional, misfolded proteins that can lead to cell death. Importantly, Hsp expression is

not restricted to stress conditions; rather, these chaperones operate continuously as a part of a dynamic network to assist in protein folding and localization under physiological conditions (Gidalevitz et al. 2011).

The expression of Hsps is orchestrated by heat shock factors (HSFs), a family of conserved DNA-binding transcription factors that mediate the HSR. In humans, this family includes HSF1, HSF2, HSF4, HSF5, and the sex chromosome-encoded HSFX and HSFY (Hästbacka et al. 2025). Of these, HSF1 is the primary regulator of the classical HSR, the functional homologue of the single HSF in yeast and invertebrates and is therefore by far the most extensively studied. HSF2 also contributes to proteostasis and developmental regulation, though in distinct physiological and pathological contexts (Gomez-Pastor et al. 2018; Joutsen and Sistonen 2019; Pessa et al. 2024).

HSF1 activation follows a chaperone titration model (Figure 3). Under non-stress conditions, HSF1 exists as an inactive monomer in the cytosol, where it is sequestered by Hsps (Hsp70 and Hsp90) and the chaperonin TCP-1 ring complex (TRiC), which repress its activation (Björk and Sistonen 2010; Neef et al. 2014). During heat shock, cellular proteins begin to unfold or denature, which can be harmful if not managed, as they may aggregate and hinder physiological cellular processes (Morimoto 2011). As Hsps become engaged in binding denatured proteins, which prevents aggregation and facilitates proper refolding, HSF1 is released from the inhibitory complexes (Silver and Noble 2012). The liberated HSF1 monomers trimerize, forming the transcriptionally competent structure that translocates into the nucleus. There, the trimer binds to specific DNA sequences known as heat shock elements (HSEs) located in the promoters of Hsp genes initiating their transcription (Joutsen and Sistonen 2019; Morimoto 2011). The HSR-based HSF1 activation is driven by temperature-dependent phase separation: above a certain threshold HSF1 forms reversible liquid condensates that raise local concentration, promote trimerization and HSE binding, and rapidly trigger heat shock gene transcription (Ren et al. 2025).

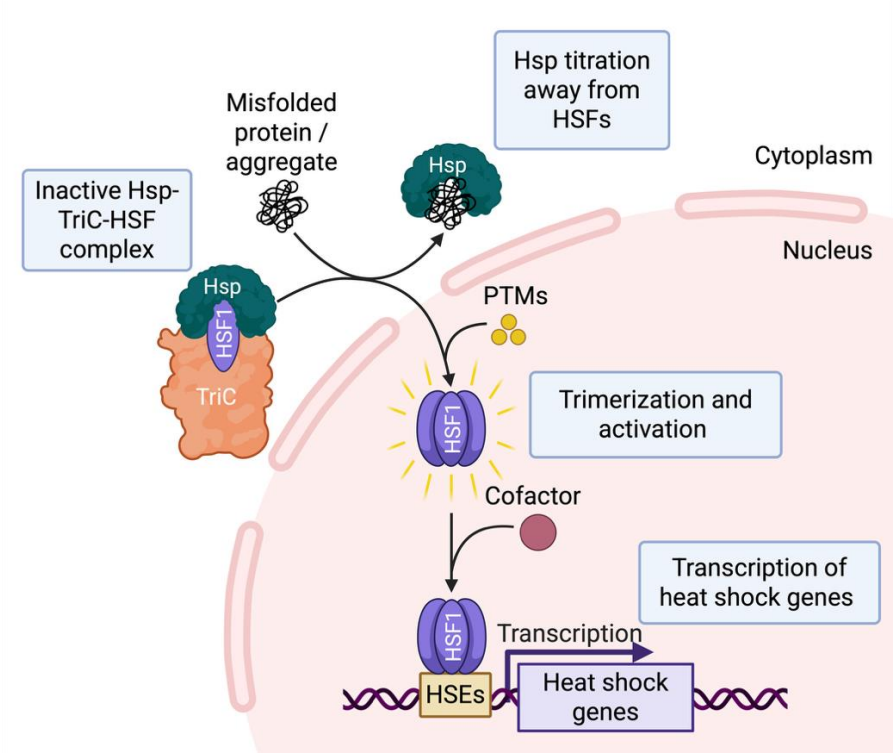

Figure 3. The HSF1 titration model of activation during the heat shock response. Under non-stressed conditions, HSF1 exists as an inactive monomer bound by heat shock proteins (Hsps) and the TCP-1 ring complex (TRiC), which repress its activation. Upon proteotoxic stress, misfolded or aggregated proteins sequester chaperones away from HSF1. This shift, together with activating post-translational modifications (PTMs), promotes HSF1 trimerization and nuclear translocation. In the nucleus, trimeric HSF1, often in cooperation with transcriptional cofactors, binds to heat shock elements (HSEs) and induces transcription of heat shock genes, enabling restoration of proteostasis.

The newly synthesized Hsps replenish the cellular chaperone pool, increasing the cell's capacity to refold or degrade denatured proteins. As proteostasis is gradually restored, Hsps re-associate with HSF1, returning it to its inactive state and completing a negative feedback loop (Kmiecik and Mayer 2022; Sivéry et al. 2016). Additionally, stress-inducible acetylation of HSF1 confers an additional level of attenuation, which inhibits its DNA-binding capacity (Westerheide et al. 2009). Therefore, the HSR operates as a transient self-regulating system that enables rapid yet reversible adaptation to proteotoxic stress.

In addition to trimerization and HSE binding, HSF1 transcriptional activity depends on chromatin-level regulation. The cofactor Strap together with the p300 acetyltransferase form a complex with HSF1 at Hsp promoters, enhancing chromatin acetylation, a mark of active chromatin, thereby facilitating robust transcription of heat shock genes (Xu et al. 2008). Loss of Strap impairs HSF1 binding and reduces cell survival under heat stress, highlighting the necessity of coactivator-mediated chromatin remodeling for effective HSF1 function (Xu et al. 2008).

Although HSFs coordinate the primary transcriptional program of the HSR, recent findings show that not all transcriptional outcomes in response to heat stress are mediated by HSFs. A parallel, HSF-independent pathway, termed stress-induced transcriptional attenuation, acts to repress nonessential gene expression during proteotoxic stress. In this process, p38 MAP kinase and negative transcription elongation factors, such as NELF, accumulate at target promoters resulting in genome-wide reduction in transcription in coordination with translational arrest and nascent-chain ubiquitination (Aprile-Garcia et al. 2019). This mechanism complements HSF-driven chaperone induction by limiting transcriptional load, emphasizing that the HSR requires both HSF-dependent activation and HSF-independent repression of target genes to restore proteostasis.

Nonetheless, given the central role of HSFs in coordinating the HSR, clarifying their structural organization provides a foundation for understanding the molecular basis for both physiological and pathological stress signaling. Crystallographic studies, where the high-resolution structure of the human HSF2 DNA-binding domain was elucidated (Feng et al. 2016; Jaeger et al. 2016), have further clarified how subtle sequence and post-translational variations contribute to functional divergence among HSF paralogs. The following section will examine the domain architecture and trimerization motifs of the general HSF paralog, focusing on structural features enabling DNA binding, oligomerization and regulatory interactions.

1.3.1 Structural organization of HSFs

The capacity of HSFs to recognize their target DNA sequences and regulate transcription is determined by their conserved modular domain architecture (Figure 4A). At the N-terminus, all HSFs contain a helix-turn-helix DNA-binding domain (DBD) that specifically recognizes the 5'-nGAAn-3' motif within HSEs (Amin et al. 1988). The spatial arrangement of these pentameric motifs influences the affinity and specificity with which different HSFs bind them (Yamamoto et al. 2009).

Trimerization of HSF1, HSF2, and HSF4 monomers is mediated by two adjacent leucine-zipper-like heptad repeats, HR-A and HR-B, which form hydrophobic coiled-coil interactions with the corresponding regions of other monomers, creating a triple-stranded leucine-zipper structure (Peteranderl et al. 1999; Rabindran et al. 1993; Yoshimura et al. 2024) (Figure 4C). In HSF1 and HSF2, an additional carboxy-terminal heptad repeat (HR-C) provides an intramolecular repression site by interacting with HR-A/B to prevent spontaneous

oligomerization under non-stress conditions (Hästbacka et al. 2025; Rabindran et al. 1993) (Figure 4B). Interestingly, HSF1 and HSF2 have been shown to form heterotrimers, the function of which remains incompletely understood but likely reflects a level of functional integration between stress-responsive and developmental transcriptional programs (Sandqvist et al. 2009). Given the shared structural homology of the HSF family, it is plausible that the other human HSF paralogs are also capable of forming heterotrimers, eliciting refined transcriptional responses with unique DBD-combinations. However, because HR-A/B trimerization motifs have been structurally characterized only for HSF1, HSF2 and HSF4, confirmation for the lesser-known paralogs will require further structural characterization to determine whether the heterotrimerization observed for HSF1 and HSF2 extends broadly across the family.

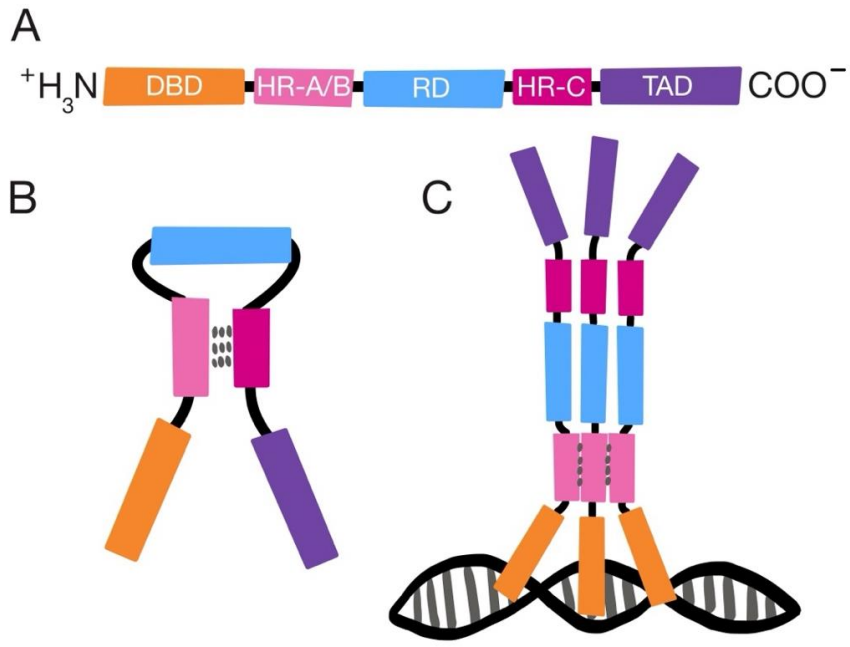

Figure 4. Conserved domain architecture and trimerization mechanism of human heat shock factors. (A) Schematic representation of the modular domains of human HSFs. All paralogs share an N-terminal DNA-binding domain (DBD, orange), followed by the heptad-repeat regions HR-A and HR-B (pink), which mediate trimerization. The central regulatory domain (RD, blue) is often targeted by PTMs to fine-tune HSF2 activity. HSF1 and HSF2 uniquely contain an autoinhibitory C-terminal HR-C region (magenta). The C-terminal transactivation domain (TAD, purple) recruits cofactors and chromatin-modifying complexes to modulate transcription. (B) Under non-stressed conditions, HR-C interacts with HR-A/B to maintain HSF monomers in an inactive, non-trimerized conformation. (C) Upon activation, three HSF monomers trimerize via HR-A/B interactions forming a triple-stranded coiled-coil structure, enabling high-affinity binding of the DBDs to heat shock elements (HSEs).

Downstream of the trimerization domain lies the regulatory domain (RD), which harbors numerous residues subject to PTMs that modulate HSF activity (Joutsen and Sistonen 2019).

However, PTMs are not confined to the RD; residues throughout the HSF monomer can undergo modifications such as phosphorylation (Guettouche et al. 2005), acetylation (Purwana et al. 2017; Raychaudhuri et al. 2014, Westerheide et al. 2009), ubiquitination (Akimov et al. 2018; Kim et al. 2016), and small ubiquitin-like modifier (SUMO) addition, also known as SUMOylation (Zhang et al. 2021). These PTMs fine-tune HSF activation by influencing its stability, DNA-binding capacity, and the duration and intensity of transcriptional output in response to specific stress stimuli.

Finally, at the C-terminus, the transactivation domain (AD) functions as a platform for cofactors and chromatin remodelers, mediating either activation or repression of HSF trimers, since trimerization alone is not always sufficient to drive target gene expression (Joutsen and Sistonen 2019; Shi et al. 1995).

These modular features – HR-A/B region, RD, and AD – are conserved in HSF1, HSF2, and HSF4, with the HR-C domain present only in HSF1 and HSF2. Among the human HSF family, the DBD is the only universally conserved domain. In contrast, HSF5, HSFX, and HSFY remain poorly characterized in comparable structural detail, and their domain organization and functional roles are yet to be elucidated (Hästbacka et al. 2025). The following chapters will explore the distinct regulatory mechanisms and functions of HSF1 and HSF2 in the contexts of stress adaptation and breast cancer invasion.

1.3.2 Heat shock factor 1

HSF1 is the prototypical member of the HSF family and the principal regulator of the HSR. Its activation follows the canonical titration mechanism previously described in Chapter 1.3, where molecular chaperones maintain HSF1 in an inactive monomeric state and release it upon proteotoxic stress. This enables rapid and reversible transcriptional activation of stress-protective genes, primarily those encoding Hsps, which restore proteostasis and attenuate further HSF1 activity through negative feedback.

In addition to transcriptional activation, HSF1 modulates epigenetic and post-transcriptional processes that fine-tune the cellular stress response. It regulates alternative cleavage and polyadenylation at stress-responsive loci to favor proteostasis-supporting isoforms and remodels chromatin through DNA methylation and looping, reinforcing transcriptional outcomes during stress adaptation (Fink et al. 2025). HSF1 activity is further sustained by co-chaperones, such as CHIP (C-terminus of Hsp70-interacting protein), which stabilize its

active form and maintain Hsp induction during prolonged stress (Dai et al. 2003). Loss of CHIP disrupts this balance, impairing cytoprotective gene expression and increasing susceptibility to apoptosis.

1.3.2.1 Physiological roles of HSF1 in development and metabolic homeostasis

HSF1 is well established as responding dynamically to proteotoxic stress; however, evidence now shows that its activity extends well beyond the canonical HSR. HSF1 exhibits constitutive activity with nuclear localization detectable in several benign human tissues (Joutsen et al. 2024). Studies in HSF1-deficient mice revealed its essential role in development, as loss of HSF1 causes prenatal lethality, female infertility, and growth retardation (Xiao 1999). These phenotypes likely reflect the broader role of HSF1 in coordinating proteostasis with cellular energy metabolism, enabling metabolic adaptation to nutrient availability (Jin et al. 2011). The evolutionarily conserved interplay between proteostasis and metabolism involves AMPK, which upon metabolic stress phosphorylates HSF1 at S121 to repress its transcriptional activity, thereby reducing expression of protein quality-control genes and increasing susceptibility to proteotoxic stress (Dai et al. 2015; Gomez-Pastor et al. 2018; Hahn and Thiele 2004).

HSF1's cytoprotective functions are also implicated in metabolic homeostasis and age-related disease. Restoration of HSF1 expression in pancreatic β-cells protects against glucolipotoxicity-induced endoplasmic reticulum stress and apoptosis, implicating HSF1 in diabetes pathogenesis (Purwana et al. 2017). Furthermore, overexpression of HSF1 in *C. elegans* promotes longevity by modulating mitochondrial turnover through ubiquilin-1-dependent mechanisms (Erinjeri et al. 2024), suggesting a conserved role in cellular homeostasis and metabolic regulation.

1.3.2.2 HSF1 in cancer and neurodegenerative disorders

In contrast to the protective functions where HSF1 ensures survival during acute stress, aberrant or chronic activation contributes to pathological conditions, including cancer and neurodegeneration (Pessa et al. 2024). A hallmark of neurodegenerative diseases is the accumulation of misfolded protein aggregates; a process directly tied to HSF1's role in proteostasis. At the molecular level, PTMs modulate HSF1 stability and activity in disease contexts. In neuroblastoma cells, acetylation at K80 promotes HSF1 destabilization by enhancing its susceptibility to ubiquitination and proteasomal degradation, thereby impairing its protective stress response and potentially contributing to neurodegenerative disease

pathology (Kim et al. 2016). Conversely, in glioblastoma cells, HSF1 SUMOylation on K298 promotes nuclear retention and protein stability, which enhances transcriptional activity, supports proliferation and migration, and decreases apoptotic susceptibility, thereby indicating a pro-oncogenic role for HSF1 (Li et al. 2024).

In cancer, HSF1 governs a broad array of cellular processes distinct from the canonical HSR, encompassing pathways related to metabolism, cell cycle regulation, DNA repair, apoptosis, cell adhesion, and extracellular matrix organization (Mendillo et al. 2012). Nevertheless, Hsp genes remain integral components of this reprogrammed network, which exhibits cancer-specific patterns of regulation. By sustaining chaperone systems, HSF1 enables cancer cells to tolerate proteotoxic and metabolic stress (Gomez-Pastor et al. 2018). Elevated HSF1 expression and nuclear accumulation are hallmarks of malignancy and correlate with poor prognosis in breast, colon, and lung cancers (Calderwood 2012; Scherz-Shouval et al. 2014). Functionally, HSF1 promotes proliferation, invasion, and survival through direct regulation of oncogenic transcriptional programs (Dai et al. 2007; Jacobs et al. 2024; Mendillo et al. 2012; Scherz-Shouval et al. 2014; Smith et al. 2022). Loss of HSF1 impairs tumor growth in cancers driven by RAS or p53 mutations (Dai et al. 2007). In hepatocarcinoma, HSF1 deletion enhances insulin and AMPK signaling, which redirects hepatic metabolism toward carbohydrate utilization and decreased lipid synthesis, creating an unfavorable metabolic environment for carcinogen-driven transformation (Jin et al. 2011). Moreover, frequent activation of HSF1 in cancer-associated fibroblasts promotes tumor progression by supporting malignant reprogramming within both cancer cells and their surrounding stroma (Scherz-Shouval et al. 2014). In breast cancer specifically, HSF1 activation under carboplatin-induced stress triggers autophagy – a cytoprotective mechanism that enhances chemoresistance – whereas HSF1 silencing impairs this response and sensitizes cells to apoptosis, increasing carboplatin efficacy (Desai et al. 2012). Similarly, by downregulating the chemokine CCL5, HSF1 impairs $CD8^+$ T-cell recruitment which suppresses antitumor immune responses in breast cancer (Jacobs et al. 2024). Together, these findings suggest that HSF1 not only promotes drug-induced stress adaptation but also facilitates immune evasion, both of which may influence therapeutic responsiveness in breast cancer.

Taken together, HSF1 functions as a master regulator of cellular proteostasis that integrates stress, metabolic, and oncogenic signaling. Its broad regulatory capacity provides a useful framework for understanding the distinct yet overlapping functions of HSF2, whose roles in EMT and breast-cancer invasion form the central focus of this thesis.

1.3.3 Heat shock factor 2

For decades after the discovery of the HSR, it was believed that a single HSF was responsible for the inducible Hsp expression in eukaryotes. However, the identification and cloning of a second, related factor in human and murine cells in 1991 revealed a more complex system (Sarge et al. 1991; Schuetz et al. 1991). The originally known HSF was subsequently renamed HSF1, and the newly identified paralog was designated HSF2. This discovery prompted the question of whether mammalian cells possess a broader family of HSFs and how their functions may diverge or overlap.

1.3.3.1 Stress-response profile of HSF2

Unlike HSF1, which is rapidly and transiently activated by acute proteotoxic stress, HSF2 displays a more developmentally regulated and stress-specific activation profile (Sistonen et al. 1994). Although often regarded primarily as a developmental factor, HSF2 is not uncoupled from the HSR (Himanen et al. 2022). Both HSF1 and HSF2 co-occupy the Hsp70 promoter during classical heat shock, with maximal promoter binding depending on intact HSF1 (Östling et al. 2007; Sistonen et al. 1994). Through this cooperation, HSF2 acts as a context-dependent co-regulator of the HSR which can modulate HSF1-driven Hsp gene expression. Yet, despite this functional overlap, their stress responses diverge significantly. Acute heat stress strongly activates HSF1 but paradoxically inactivates HSF2 through solubility changes that promote its nuclear export (Mathew et al. 2001). Moreover, unlike HSF1, which is inactivated by high Hsp levels through a negative feedback loop (Figure 3), HSF2 is stabilized by elevated Hsp levels: in thermotolerant cells that have accumulated Hsps, HSF2 remains soluble and transcriptionally competent (Mathew et al. 2001). However, under prolonged proteotoxic stress, HSF2 becomes increasingly activated and supports cell survival not by enhancing chaperone induction but by maintaining cadherin-mediated cell-cell adhesion (Joutsen et al. 2020).

1.3.3.2 Regulation of HSF2 abundance and activity

HSF1 is widely expressed and tightly regulated through a wide array of PTMs that modulate its activation, DNA binding, and attenuation. In contrast, HSF2 activity is controlled predominantly through its protein stability and abundance, with PTMs mainly influencing its turnover. In the murine prenatal neocortex, HSF2 is stabilized through acetylation by histone/lysine acetyl transferases CBP or EP300, and dominant mutations in these enzymes correspond to decreased HSF2 levels and altered expressions of stress-responsive chaperones

in patient-derived cells (De Thonel et al. 2022). Conversely, the lysine deacetylase HDAC1 acts as a negative regulator of HSF2: its deacetylation promotes HSF2 polyubiquitination and proteasomal degradation, thereby lowering HSF2 stability under both basal and stress conditions (Daupin et al. 2025).

Increased HSF2 levels promote its nuclear localization and transcriptional activation, indicating that HSF2 is activated by elevated intracellular concentration rather than by external stress (Sandqvist et al. 2009). Consistent with this, HSF2 is a short-lived, labile protein subject to rapid degradation through the ubiquitin-proteasome pathway (Ahlskog et al. 2010; Mathew et al. 1998). Inhibition of proteasomal degradation, for example by hemin, preferentially stabilizes HSF2 over HSF1, leading to the accumulation of HSF2, which induces a subset of Hsp genes (Kawazoe et al. 1998; Mathew et al. 2001). This suggests that cells can differentially modulate HSF1 and HSF2 activation depending on the nature of the stress (Mathew et al. 2001). Together, these regulatory features show that HSF1 and HSF2 can be co-activated under certain proteotoxic or metabolic stresses, but in other contexts only one paralog predominates, reflecting a division of labor in the stress response (Sistonen et al. 1994). As such, HSF2 responds to a narrower spectrum of stressors than HSF1 and contributes primarily to prolonged or differentiation-associated stress responses (Abane and Mezger 2010).

1.3.3.3 Structural and mechanistic regulation of HSF2

The mechanistic differences are further reflected in the structural organization and regulatory interactions of HSF2. Both HSF1 and HSF2 bind DNA as trimers (Figure 4C), but inactive HSF2 exists predominantly as a dimer rather than a monomer as in HSF1, reflecting distinct modes of control (Sistonen et al. 1994). Moreover, HSF2 can autoregulate its own expression through binding to an HSE within its promoter, functioning as a negative feedback mechanism (Park et al. 2015). Co-expression of HSF1 and HSF2 exerts a stronger repressive effect than either factor alone, indicating that heteromeric HSF1-HSF2 interactions fine-tune HSF2's transactivation capacity under both stress and non-stress conditions.

Despite decades of biochemical characterization, structural information on mammalian HSFs has been limited. In 2016 two independent groups reported the first crystal structures of the human HSF2-DBD, resolving it at high-resolution both in its isolated form (1.32 Å) (Feng et al. 2016) and bound to HSEs (1.73 Å) (Jaeger et al. 2016), establishing a foundation for understanding its paralog-specific DNA recognition and PTM regulation. Inspection of HSF2-

DNA complexes revealed unique sequence motifs within the DBD that accommodate specific PTMs and cofactor interactions, underlying its distinct transcriptional behavior compared with HSF1 (Jaeger et al. 2016). One of these characterized PTMs within the DBD is SUMOylation at K82, which inhibits HSF2-DNA interactions through steric and electrostatic interference, without altering trimerization, thus hindering its access to HSEs (Tateishi et al. 2009).

1.3.3.4 *HSF2* gene and promoter architecture

The human *HSF2* gene, located on chromosome 6, spans approximately 33 kb and contains 13 exons transcribed from multiple start sites within a GC-rich, TATA-less promoter region (Nykänen et al. 2001). Functional analysis of the 5' regulatory region revealed that both 450-bp and 950-bp fragments upstream of the *HSF2* transcription start site (TSS) drive strong luciferase reporter activation. Reversal of these sequences markedly reduced (450 bp) or abolished (950 bp) reporter activity, demonstrating that the *HSF2* promoter is orientation dependent (Nykänen et al. 2001). Furthermore, a broader 1.5-kb upstream region was later implicated in HSF2 autoregulation (Park et al. 2015), suggesting that additional regulatory elements may lie beyond 950 bp. However, because no other regions were tested, it remains unclear whether the additional 550 bp contain functional motifs or simply flank the regulatory elements within the 950-bp region. Therefore, as longer upstream sequences were not examined, the full extent of the *HSF2* promoter remains undetermined and could extend beyond 1.5 kb.

1.3.3.5 Tissue-specific expression and developmental functions of HSF2

HSF2 expression is highly tissue- and stage-specific (Fiorenza et al. 1995; Joutsen et al. 2024), likely regulated through transcriptional, post-transcriptional, and proteolytic mechanisms, including regulated alternative splicing that modulates transcriptional activity in a tissue-dependent manner (Goodson et al. 1995). During embryogenesis, HSF2 shows stage-specific expression, with DNA-binding activity correlating with increased protein levels, which suggests concentration-dependent activation (Min et al. 2000; Rallu et al. 1997). In the testis, where HSF2 expression is highest, the factor is constitutively active and regulates genes involved in differentiation and chromatin remodeling (Björk et al. 2010; Goodson et al. 1995; Sarge et al. 1994). During spermatogenesis, HSF2 expression oscillates in a cell- and stage-specific pattern (Björk et al. 2010; Sarge et al. 1994). HSF2-deficient mice exhibit neurological and reproductive abnormalities, including reduced testis and epididymis size,

altered seminiferous tubule morphology, defective spermatogenesis, and abnormal sperm chromatin organization (Abane and Mezger 2010; Åkerfelt et al. 2008; Kallio 2002; Wang et al. 2003). Collectively, these observations demonstrate that precise control of HSF2 expression is required for proper development and differentiation.

1.3.3.6 HSF2 in cellular plasticity and cancer

Beyond development, HSF2 has gained attention for its role in epithelial plasticity and cancer progression. Recent evidence indicates that HSF2 cooperates with HSF1 to sustain oncogenic transcriptional programs that extend beyond classical heat shock targets, including genes involved in proliferation, metabolism, and proteostasis (Smith et al. 2022). Despite their divergent responses to thermal stress, HSF1 and HSF2 occupy largely overlapping chromatin sites in cancer cells, with functional differences likely arising from distinct cofactor interactions (Smith et al. 2022). Due to its short half-life and rapid turnover, HSF2 may provide tumor cells with a flexible mechanism to adjust gene expression to the proteotoxic demands of rapid growth. In prostate cancer, HSF2 acts as a suppressor of invasion as its downregulation coincides with EMT activation and enhanced invasiveness (Björk et al. 2016). Similarly, in human breast cancer cells, TGF-β-induced EMT requires HSF2 downregulation, which promotes an invasive phenotype, whereas enforced HSF2 expression drives proliferation while limiting migratory potential (Pessa et al. 2025). These findings are suggestive of HSF2 acting as a mediator of a switch-like balance between proliferative and invasive phenotypes (Pessa et al. 2025). Consistent with this role, HSF2 maintains expression of multiple cadherin superfamily genes under prolonged proteotoxic stress, thereby preserving cadherin-mediated cell-cell adhesions (Joutsen et al. 2020). Because the loss of E-cadherin is characteristic in EMT (Xie et al. 2004), these findings further support the notion that HSF2 contributes to the maintenance of epithelial identity.

Altogether, these observations position HSF2 as a potential component of the metastatic cascade; therefore, its role in malignant transformation should be investigated in more detail. However, the molecular mechanisms by which TGF-β suppresses HSF2 remain unknown. Specifically, it is unclear which TFs are recruited to the *HSF2* promoter, and which cis-regulatory elements mediate this repression. Clarifying the mechanisms by which TGF-β signaling represses HSF2 may reveal how stress and developmental pathways intersect to promote epithelial plasticity and invasion in breast cancer progression. Addressing these unresolved aspects of HSF2 regulation forms the focus of this thesis.

2 Aims

Breast cancer is now the most diagnosed cancer worldwide, accounting for around 2.3 million new cases in 2022 (Kim et al. 2025). Despite recent advancements in diagnostic tools including circulating tumor DNA biomarkers (Bartolomucci et al. 2025) and artificial intelligence (AI)-assisted cancer detection from medical imaging (Sechopoulos et al. 2021), metastatic spread remains a major clinical challenge and the leading cause of mortality in solid tumors (Dillekås et al. 2019; Kennecke et al. 2010). This is partly due to the asymptomatic nature of early-stage disease, limitations in current screening strategies, and the aggressive biology of certain cancers that enables early dissemination before detection. Given that the 5-year relative survival rate declines sharply from 100% in localized breast cancer to 32.6% in cases with distant metastases (National Cancer Institute 2025), understanding the mechanisms that drive the acquisition of invasive traits is important.

Despite the well-established role of EMT in cancer progression, the molecular regulators of this process remain incompletely characterized. HSF2, a TF traditionally linked to cellular stress responses, has recently emerged as a potential modulator of invasive behavior in breast cancer. Pessa and coworkers (2025) discovered that TGF-β signaling mediates HSF2 suppression, which occurs concomitantly with EMT in breast cancer cells. Furthermore, they demonstrated that forced ectopic overexpression of HSF2 in breast cancer cells cultured as spheroids results in rapid proliferation but an inability to form invasive structures, in contrast to wild-type cells that readily develop invasive structures characteristic of EMT. These findings suggest that HSF2 suppression is functionally linked to invasive phenotypes.

This thesis aims to elucidate the regulatory mechanisms underlying TGF-β-induced suppression of HSF2, which occurs simultaneously with EMT in breast cancer cells. Preliminary unpublished data from the Sistonen laboratory indicate that TGF-β signaling downregulates HSF2 through transcriptional mechanisms involving the 5'UTR of the *HSF2* promoter. To investigate further, the following objectives were established: (1) definition of the specific region within the 5'UTR containing the relevant TF binding site(s), and (2) identification of the TF(s) mediating the TGF-β-driven downregulation of HSF2. The first objective was addressed using truncated *HSF2* promoter constructs and luciferase reporter assays. For the second objective, a DNA affinity purification approach was designed and piloted to identify candidate TFs.

3 Materials and methods

3.1 Cell lines, culture conditions, and treatments

The human triple negative breast cancer cell line HS578T, which lacks estrogen, progesterone and human epidermal growth factor receptors, was used in this study. Cells were maintained in Dulbecco's Modified Eagle's Medium (DMEM, Gibco) supplemented with 10% heat-inactivated fetal bovine serum (FBS, Serena), 1 U/ml penicillin (Sigma-Aldrich), 100 µg/ml streptomycin (Sigma-Aldrich), and 10 µg/ml insulin (Gibco) in a humidified atmosphere at 37°C with 5% CO_2. Cells were routinely tested for Mycoplasma.

Assay media composed of DMEM supplemented with 2% FBS and 10 µg/ml insulin was used for control treatments. TGF-β treatments contained 10 ng/ml TGF-β (R&D Systems) in assay media. For actinomycin D (ActD) chase experiments, ActD treatments consisted of 10 µg/ml in assay media either alone or in combination with 10 ng/ml TGF-β.

3.2 Plasmids

Jenny Pessa (Åbo University) kindly provided plasmids consisting of a firefly luciferase validation vector backbone (Addgene plasmid #99297) containing an ampicillin resistance gene and luciferase reporter gene (*luc*) (Figure S1A-C). In these plasmids, the luciferase gene was under the control of either a *MMP9* promoter with four Smad-binding elements (MMP9-4xSBE) or various *HSF2* promoter inserts that are visualized in Figure 5. Additionally, commercial plasmids coding for β-galactosidase under the regulation of the simian virus 40 promoter were utilized for normalization purposes in luciferase assays (Figure S1D).

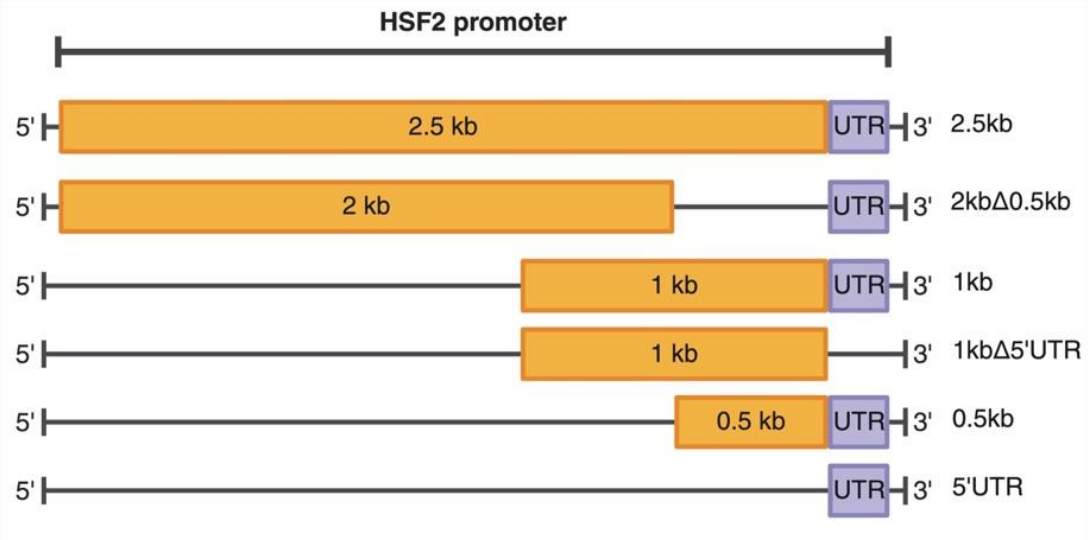

Figure 5. Schematic representation of *HSF2* promoter inserts cloned into luciferase reporter plasmids.

3.3 Primer design

By utilizing the JASPAR online database, the sequence of the *HSF2* promoter's 5'UTR region (192 bp) was cross-referenced with all known human TF binding motifs, identifying four potential TF binding sites within the 5'UTR region with a specificity exceeding 98%.

TakaraBio Primer Design Tool was utilized to design primers. For luciferase assays, deletion plasmid (ΔDel1–4) primers (listed in Table 1) were designed to generate constructs missing specific regions within the 5'UTR, each containing a potential TF binding site, as visualized in Figure 6. Additionally, 5-bp overhangs were designed into the primers, enabling homologous recombination in construct generation following linearization.

Table 1. Primers used for *HSF2* promoter's 5'UTR deletion plasmid generation. +: forward primer, -: reverse primer.

Target	*Strand*	*Primer sequence*	*Product size (bp)*
ΔDel1	+	5'-GCCGGAGAGGCCTCTCGGCCTTGCCG-3'	4126
	-	5'-AGAGGCCTCTCCGGCTTCAAAATCCCTTAACG-3'	
ΔDel2	+	5'-GGCCGCCCCGCCTGCGTTGTGGGCGTTCTCG-3'	4090
	-	5'-GCAGGCGGGGCGGCCGCACGTGACG-3'	
ΔDel3	+	5'-CCGCGTTCGCCACCATGGAAGATGCC-3'	4114
	-	5'-TGGTGGCGAACGCGGTGGTAGCGGC-3'	
ΔDel4	+	5'-ATCTGCTGGGGTGTAGAATTTGGAATCCCTGC-3'	4084
	-	5'-TACACCCCAGCAGATCTTGGTCCCCG-3'	

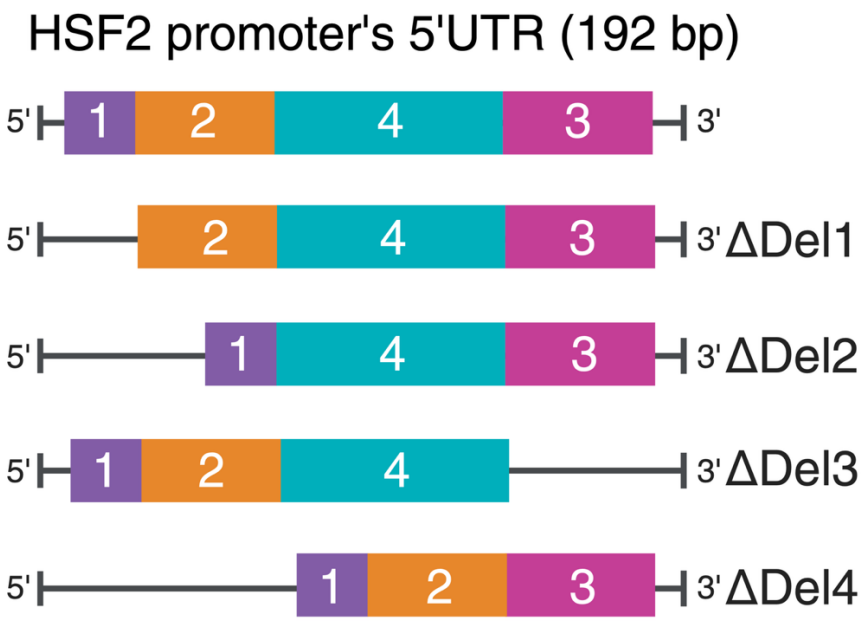

Figure 6. Schematic representation of the *HSF2* promoter's 5'UTR deletion plasmid inserts.

For DNA affinity purification (DAP), 5'-biotinylated DNA probe primers were designed to amplify 144–145 bp segments of the *HSF2* promoter's 0.5-kb region (probes 1–5), the plasmid backbone (negative control), and an area of the MMP-promoter together with SBEs (positive control), with reverse primers biotinylated at the 5'-end (Table 2).

Table 2. Primers used for DNA probe generation by PCR. +: forward primer, -: reverse primer.

Target	*Strand*	*Primer sequence*	*Product size (bp)*
Probe 1	+	5'-ACAGTTTTAAGTAATCGAGAGTGA-3'	145
	-	5'-[BIO]ATGATGTGCTAGGCCCCAAA -3'	
Probe 2	+	5'-TCATTATTTTTAAGACAATTTCAA-3'	144
	-	5'-[BIO]CCTTCAGGGCCTTTGAGT -3'	
Probe 3	+	5'-ACCACACTTTGCCTGCCAAACT-3'	144
	-	5'-[BIO]GCCTTGATGGTAGCAGACTTAG -3'	
Probe 4	+	5'-ATCCAAACACGGTCTCCCAAGC-3'	144
	-	5'-[BIO]AGAGAAAAGCGATTGGCTGCTG-3'	
Probe 5	+	5'-GCTCCCACCCCCTTCATGTCAGCA-3'	144
	-	5'-[BIO]GCGGCCGCACGTGACGGACA-3'	
Pos	+	5'-AGATTCAGGGCCAGGTATGGTG-3'	144
	-	5'-[BIO]GTCTGACGCTCAGTGGAACGAA-3'	
Neg	+	5'-GACAACACCGCGGCCAACTTAC-3'	144
	-	5'-[BIO]ACGCTCGTCGTTCGGTATGGCT-3'	

All utilized plasmids underwent long-read whole plasmid sequencing (Eurofins Genomics) to ensure plasmid integrity. Additionally, constructed deletion plasmids and DNA probes underwent short-read Sanger sequencing (Mix2Seq, Eurofins Genomics) targeting the inserts.

3.4 DNA amplification and extraction from agarose gels

Four *HSF2* promoter 5'UTR deletion luciferase expression plasmids (ΔDel1–4) were generated by PCR using the Phusion Plus Kit (Thermo Scientific) according to the manufacturer's instructions. The PCR reactions utilized the GC enhancer provided in the kit and 10 ng of 5'UTR plasmid DNA as template. The temperature protocol was as follows: 98°C for 30 s, 25 cycles of 98°C for 10 s, 60–70°C gradient for 10 s, 72°C for 1 min, and a final extension at 72°C for 5 min.

For DAP, seven 5'-biotinylated DNA probes – probes 1–5 along with negative and positive controls – were generated by PCR using the Taq DNA Polymerase Kit (New England Biolabs) with minor modifications to the manufacturer's protocol. For probe 5 and the control

probes, primer concentration was 200 nM, whereas probes 1–4 required 400 nM primers for efficient amplification. In addition, the $MgCl_2$ concentration was adjusted to 2 mM for probes 1–4. Each reaction contained 1 ng of template DNA: the 2.5-kb plasmid containing the full *HSF2* promoter served as the template for probes 1–5 and the negative control probe, while the MMP9 plasmid was used as the template for the positive control probe.

For probe 5 and the control probes, PCR amplification was performed under the following conditions: an initial denaturation at 95°C for 3 min, followed by 32 cycles of denaturation at 95°C for 20 s, annealing at 58°C for 20 s, and extension at 68°C for 30 s, with a final extension step at 72°C for 5 min. For probes 1–4, amplification was carried out with a modified protocol consisting of an initial denaturation at 95°C for 30 s, followed by 32 cycles of 95°C for 20 s, annealing at probe-specific temperatures for 20 s, and extension at 68°C for 30 s, with a final extension at 72°C for 5 min. The annealing temperatures were 56.6°C for probe 1, 52.8°C for probe 2, 60.3°C for probe 3, and 58°C for probe 4.

Methylated bacterial template DNA was digested with 20 U of Dpn1 restriction enzyme per 50 µl PCR reaction at 37°C for 1 h, followed by enzyme inactivation at 80°C for 20 min. The PCR products were loaded with Purple Gel Loading Dye, No SDS (New England Biolabs) and separated by agarose electrophoresis on a 1–2% (w/v) agarose gel (TAE, Midori Green) at 60–100V. GeneRuler 1 kb Plus (Thermo Fisher Scientific) and 100-bp Penn State DNA ladders were used for size estimation. Gels were imaged with iBright CL1500 (Thermo Fisher Scientific), the DNA bands excised, and DNA purified using the NucleoSpin® Gel and PCR Clean-up kit (Macherey-Nagel), according to the manufacturer's instructions. DNA concentrations were determined using the Qubit™ dsDNA Quantification Assay Kit (Thermo Fisher Scientific).

3.5 In-fusion cloning of *HSF2* promoter constructs

The In-Fusion® HD Cloning Kit (Takara Bio) and its manufacturer's instructions were employed to ligate 100 ng of purified linearized plasmid DNA (ΔDel1–4) and transform stellar competent *E. coli* JM109 cells with 25 ng of ligated plasmid DNA. Deviating from the protocol, glucose-rich NZCYM media was used, and the bacterial transformations were incubated at 37°C for 1 h, at 200 rpm. A tenth of the transformation reactions were spread plated onto 1% Luria broth (LB) agar plates containing 50 µg/ml ampicillin and grown overnight at 37°C. Plasmid DNA was amplified by inoculating 500 ml LB media cultures (50 µg/ml ampicillin) with individual bacterial colonies and grown overnight. The plasmid DNA

was isolated and concentrated using NucleoBond® Xtra Maxi Plus Kit (Macherey-Nagel), following the manufacturer's instructions.

3.6 Transfection parameters

Transient transfections were conducted using the Neon Transfection System (MPK5000, Invitrogen), in accordance with the manufacturer's instructions with slight modifications. For electroporation, 2×10^6 HS578T cells were suspended in 100 µl of Buffer R with 15 µg of luciferase plasmid DNA and 5 µg of β-galactosidase plasmid DNA and pulsed three times at 1050 V for 20 ms. For the luciferase assays, 2×10^4 transfected cells per well were seeded into 96-well plates in triplicate, while the remaining cells were evenly divided between two ⌀60 mm plates, for β-galactosidase assays. Transfected cells were allowed to recover for 24 h before treatment.

3.7 Luciferase assay

The control and TGF-β-treated HS578T cells (4 h for the MMP9 positive control sample, 24 h for *HSF2* promoter samples) were lysed with the Britelite™ Plus luciferase assay reagent (Revvity) according to the manufacturer's instructions. Firefly luciferase activity was measured using the Hidex Sense Microplate Reader, with a 1-second luminescence infrared cutoff. For the β-galactosidase assays, the untreated and TGF-β-treated cells were harvested and lysed with passive lysis buffer (Promega) for 15 min at room temperature (RT), followed by centrifugation at 15000 × g for 1 min at 4°C. The β-galactosidase activity was measured from supernatants mixed at a 3:200 ratio with ONPG buffer (81 mM $Na_2HPO_4 \cdot 2\ H_2O$, 18 mM NaH_2PO_4, 4 mg/ml ONPG [o-nitrophenyl-β-D-galactopyranoside], 5 mM 2-mercaptoethanol, 1 mM $MgCl_2$). The assays were conducted in triplicate for three independent biological replicates, following a 30 min incubation at 37°C, with measurements taken using the Hidex Sense Microplate Reader at OD_{420} with 25 flashes.

Luciferase activity data were first normalized to β-galactosidase activity for each sample, then to the corresponding control group, yielding control values of 1 and treatment values as fold change. The mean fold change was then calculated across three (or six for 1kbΔ5'UTR; 5'UTR and MMP9 constructs) independent experimental replicates.

3.8 Nuclear extract preparation

For subcellular fractionation, multiple buffer compositions and protocols were tested during initial method development to optimize nuclear extract preparation, including the commercial

fractionation kit NE-PER™ (Thermo Fisher Scientific) with its accompanying protocol. The tested buffer formulations are listed in the supplementary Table S1 and Table S2. The final protocol was selected based on cost-efficiency, extract yield, and nuclear purity, as assessed by protein quantification and marker analysis.

HS578T cells were treated either with control or TGF-β treatments for 24 h, followed by harvesting by trypsinization. Several nuclear extraction strategies were tested during method development, and the final optimized protocol was as follows. Cells were resuspended in nuclear extraction buffer (10 mM Tris-HCl pH 7.9, 3 mM $CaCl_2$, 2 mM $MgCl_2$, 0.1% Triton X-100, supplemented with 0.5 mM DTT and protease inhibitors) at a ratio of 1×10^6 cells per 1 ml buffer, and incubated on ice for 5 min. Mechanical disruption was performed by 20 strokes with a Dounce homogenizer, and membrane rupture was confirmed by DAPI staining.

To separate cytoplasmic and nuclear compartments, nuclei were pelleted by centrifugation at 1000 × g for 5 min at 4°C, washed twice with PBS, and lysed in RIPA buffer (Pierce™ Thermo Scientific), supplemented with 0.5 mM DTT and protease inhibitors, for 30 mins with rotation at 4°C. DNA digestion was performed by sonication using the Bioruptor® Plus (Diagenode) for 10 cycles (15 s/30 s ON/OFF). Cellular debris was removed by centrifugation at 20817 × g for 10 min at 4°C.

Cytoplasmic fractions, which were initially dilute, were concentrated using a SpeedVac to facilitate downstream protein analysis. However, this resulted in elevated salt concentrations that impaired SDS-PAGE resolution. Therefore, cytoplasmic proteins were instead recovered by cold acetone precipitation according to a publicly available protocol (Thermo Fisher Scientific 2009).

To confirm successful fractionation, proteins from whole-cell lysates, cytoplasmic, nuclear, chromatin, and debris fractions were separated by SDS-PAGE and analyzed by immunoblotting. Antibodies against nuclear marker lamin A/C, chromatin marker histone H4, cytoplasmic marker α-tubulin, and phosphorylated Smad2 (p-Smad2) as an indicator of successful TGF-β treatment, were used for validation.

3.9 DNA affinity purification

Unspecific signal was blocked from DNA probes with sonicated salmon sperm (100 µg/ml) by rotation for 15 min at RT. 1 µg of DNA probes per 1 mg of pre-cleared nuclear extracts were mixed by rotation for 30 min at RT. Equilibrated streptavidin C1 coated Dynabeads™

(Thermo Fisher Scientific) were added to samples and incubated for 10 min at RT. Facilitated by magnetic separation, beads were washed eight times with bead washing buffer (20 mM HEPES-KOH, 1.5 mM MgCl2, 0.2 mM EDTA, 0.05% NP40, pH 7.9 with and without 150 mM NaCl). To verify the pull-down, bound proteins were eluted with Laemmli buffer at 95°C for 5 min. Eluates, along with 25 µg of nuclear extracts, were analyzed by a total protein stain and immunoblotting for p-Smad2 and HSF1.

3.10 Immunoblotting

Protein samples were denatured in Laemmli buffer by boiling for 5 min, followed by separation using sodium dodecyl sulfate-polyacrylamide gel electrophoresis (SDS-PAGE) on 4-20% Mini-PROTEAN® TGX Stain-Free™ Precast gels (Bio-Rad). Precision Plus Protein Dual Color (Bio-Rad) served as the molecular weight marker. Electrophoresis was conducted at 200 V for 30 min in SDS running buffer (25 mM Tris, 192 mM glycine, 0.1% SDS, pH 8.3). Proteins separated by SDS-PAGE were transferred onto Amersham™ Protran 0.45 µm nitrocellulose membranes (Cytiva) using the Trans-blot Turbo Transfer System (Bio-Rad) at 25 V for 10 min. Unspecific signals from membranes were blocked with blocking buffer (5% milk-PBS + 0.3% TWEEN 20) for 1 h at RT. Membranes were incubated with 1° antibodies overnight at 4°C and subsequently with their corresponding horseradish peroxidase (HRP)-conjugated 2° antibodies for 1 h at RT (Table 3). 1° antibodies were diluted in 0.5% BSA in PBS with 0.02% NaN_3 and 2° antibodies in blocking buffer. Membranes were washed between incubations with washing buffer (PBS + 0.3% TWEEN 20) to remove unbound proteins. For protein detection with chemiluminescence, membranes were incubated in Amersham™ ECL Western Blotting Detection Reagents (Cytiva) and imaged using iBright CL1000.

Table 3. Antibodies utilized in immunoblotting. mAb = monoclonal antibody, pAb = polyclonal antibody, IgG = immunoglobulin G, HRP = horseradish peroxidase.

1° antibody	*2° antibody*
Anti-HSF1 mAb IgG1 (10H8, StressMarq Biosciences), 1 µg/ml	Anti-Rat IgG HRP conjugate (ab97057, abcam), 1:3000
Anti-p-Smad2 Ser465/467 (138D4) mAb IgG (#3108, Cell Signaling Technology) (60 kDa), 1:1000	Anti-Rabbit IgG HRP conjugate (W401B, Promega), 1:10000
Anti-lamin A/C pAb (#ab26300, abcam), 1:1000	Anti-Rabbit IgG HRP conjugate (W401B, Promega), 1:10000
Anti-lamin A/C (4C11, Cell Signaling Technology) 1:1000	Anti-Mouse IgG HRP conjugate (W4021, Promega), 1:10000

1° antibody	*2° antibody*
Anti-histone H4 (62-141-13) mAb IgG (#05-858, Millipore), 1:1000	Anti-Rabbit IgG HRP conjugate (W401B, Promega), 1:10000a
Anti-α-tubulin (12G10) mAb IgG (AB_ 1157911, DSHB), 1:1000	Anti-Mouse IgG HRP conjugate (W4021, Promega), 1:10000

3.11 Whole protein staining

To visualize all proteins after SDS-PAGE, polyacrylamide gels were stained with GelCode® Blue Stain Reagent (Thermo Scientific) according to the manufacturer's instructions. Gels were imaged using iBright CL1000.

3.12 Actinomycin D chase experiment and qRT-PCR

HS578T cells were seeded in 6-well plates at a density of 6×10^5 cells per well and allowed to adhere overnight. ActD, alone or in combination with TGF-β, was applied for 1, 2, 4, 6, or 8 h. Control sample cells were lysed at timepoint 0. At each timepoint, cells were lysed directly in the wells, and total RNA was extracted using the RNeasy Plus Mini Kit (Qiagen). Complementary DNA (cDNA) synthesis was performed from 1 µg of RNA using the iScript cDNA Synthesis Kit (Bio-Rad).

Quantitative real-time PCR (qRT-PCR) was performed using PowerUp™ SYBR™ Green Master Mix (Applied Biosystems) on a QuantStudio 3 instrument, with primers targeting *HSF2*, *HSPA1A* (Hsp70), and the housekeeping gene *18S* (primer sequences in Table 4). *HSF2* and *Hsp70* mRNA levels were normalized to *18S* and then to the 0-h timepoint to obtain fold-change values. Mean values were calculated from three independent biological replicates.

To assess mRNA stability, normalized qRT-PCR data were fitted using nonlinear regression to a one-phase exponential decay model:

$$Y = (Y_0 - plateau) \times e^{-Kt} + plateau,$$

where y_0 is the initial mRNA level at the first time point, *plateau* is the residual transcript level after degradation, K is decay rate constant, and t is time. From the fitted curve the half-life ($t_{1/2}$) was calculated as:

$$t_{1/2} = \frac{\ln(2)}{K}.$$

Curve fitting was performed separately for each treatment condition. The 0- and 1-h timepoints were excluded from the model to focus on the decay phase, as early transcript levels showed transient induction rather than degradation. This exclusion was applied across all transcripts and their treatments for consistent data treatment.

Table 4. Primers used for qRT-PCR. +: forward primer, -: reverse primer.

Target	*Strand*	*Primer sequence*
HSF2	+	5'-GGAGGAAACCCACACTAACG-3'
	-	5'-ATCGTTGCTCATCCAAGACC-3'
Hsp70	+	5'-GCCGAGAAGGACGACTTTGA-3'
	-	5'-CCTGGTACAGTCCGCTGATGA-3'
18S	+	5'-GCAATTATTCCCCATGAACG-3'
	-	5'-GGGACTTAATCAACGCAAGC-3'

3.13 Statistical analysis

Internal normalizations were performed in Excel (Microsoft), and statistical analyzes were conducted using GraphPad Prism 10.3.1 and R 4.5.1. Statistical significance was defined as $p < 0.05$. For luciferase assays, raw luciferase activity was first normalized to β-galactosidase to control for transfection efficiency. Two complementary analyses were performed. First, β-galactosidase-normalized luciferase values from control and TGF-β-treated samples were compared directly using paired one-tailed Student's t-tests, testing for repression in all constructs except the MMP9 positive control, for which activation was tested (Script S1). Second, to assess relative promoter responsiveness, the same normalized values were further normalized within each biological replicate to the corresponding untreated control, yielding fold-change values (TGF-β/Control). These fold-change values were analyzed using one-sample, one-tailed t-tests (Script S2). To account for multiple comparisons across constructs, p-values were corrected using the Benjamini-Hochberg false discovery rate (FDR) ($Q = 0.05$). Further pairwise comparisons between promoter constructs were performed using one-tailed Welch's t-tests to assess whether deletion of specific promoter regions resulted in a significant reduction in basal activity or TGF-β-induced repression.

For the ActD chase experiment, qRT-PCR data were analyzed in GraphPad Prism using a two-way ordinary ANOVA to assess the effects of time and treatment (ActD vs. ActD + TGF-β) on the rate of mRNA decay. Additionally, for *HSF2* mRNA levels, Dunnett's post-hoc test was applied to compare each time point to the 0-h baseline.

3.14 Statement on the use of artificial intelligence

The AI language-model tool ChatGPT5 (OpenAI) was used in this thesis solely as a supportive writing aid, in accordance with the University of Turku's guidelines for AI use in theses. The tool was employed to assist in designing the structural framework, improving clarity and academic style, and checking grammar. Examples of use include verifying the consistency of terminology and formatting, identifying potential grammatical issues, and receiving structural suggestions for organizing chapters. In all cases, the scientific content, interpretations, and final wording were produced by the author: no AI-generated content is presented as original work.

4 Results

4.1 TGF-β induces the reduction of *HSF2* transcript levels

Recent work has shown that *HSF2* mRNA levels decrease markedly after 24 h of TGF-β treatment, indicating potential transcriptional repression (Pessa et al. 2025). To corroborate these observations, HS578T cells were treated with TGF-β for 8 and 24 h; the 8-h timepoint was included to test whether HSF2 repression precedes the previously reported 24-h response and to capture potential early transcriptional changes following TGF-β stimulation. After treatment total RNA was isolated. Because qRT-PCR quantifies gene expression by amplifying DNA rather than RNA, the extracted RNA was reverse-transcribed into cDNA. This conversion preserves the relative abundance of each transcript in the sample and allows the use of gene-specific primers to accurately measure HSF2 expression across treatment conditions.

Transcript levels of *HSF2* and *Hsp70* were quantified by qRT-PCR, using *18S* rRNA as the internal reference gene to control for variation in RNA input and reverse-transcription efficiency. To account for biological variability, transcript levels were further normalized within each replicate by setting the untreated control (0 h) values to 1. Expression at 8 h and 24 h was therefore calculated as fold change relative to the corresponding baseline sample, enabling direct comparison of TGF-β-induced transcriptional changes across timepoints.

TGF-β significantly reduced *HSF2* transcript levels at both 8 h and 24 h (Figure 7). The repression was stronger at 8 h (59.7 ± 16.9%, $p < 0.05$) than at 24 h (83.9 ± 3.0%, $p < 0.01$), suggesting that maximal transcriptional suppression occurs early after stimulation. A partial recovery at 24 h may reflect attenuation of the TGF-β-dependent signal within the 8–16 h interval, consistent with the known decline of TGF-β bioactivity during prolonged incubation in culture media (Zi et al. 2011). In contrast, *Hsp70* transcript levels remained unchanged at both timepoints, indicating that TGF-β does not modulate its expression.

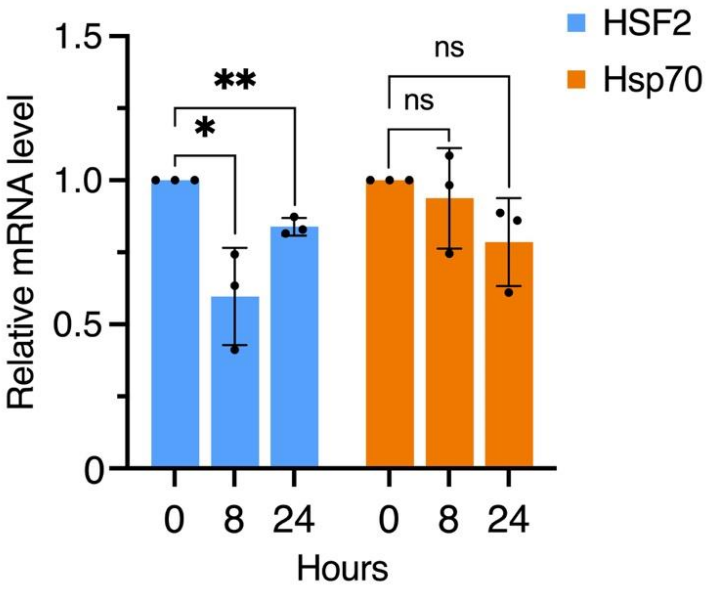

Figure 7. Relative expression of *HSF2* and *Hsp70* mRNA following 8 h and 24 h of TGF-β treatment, measured by qRT-PCR. *HSF2* mRNA levels were significantly reduced at both 8 h ($p < 0.05$) and 24 h ($p < 0.01$), compared to baseline, whereas *Hsp70* mRNA levels exhibited no significant change. Data were normalized first to *18S* rRNA and then within each replicate to the corresponding 0-h control. Data represent the mean fold change ± SD (n = 3). Statistical significance was assessed using one-sample t-tests: one-tailed for *HSF2* (testing for repression), and two-tailed for *Hsp70* (testing for either repression or induction). ns: $p > 0.05$; *: $p < 0.05$; **: $p < 0.01$

4.2 TGF-β suppresses HSF2 via transcriptional mechanisms independent of mRNA degradation

To investigate whether the reduction in *HSF2* mRNA levels upon TGF-β treatment results from transcriptional repression or accelerated mRNA degradation, HS578T breast cancer cells were treated with a well-established transcriptional inhibitor ActD, either alone or in combination with TGF-β, over a time course of 0–8 h. ActD halts *de novo* RNA synthesis, enabling the measurement of transcript stability in the absence of ongoing transcription, by monitoring decay kinetics (Lai et al. 2019). Cells treated with ActD alone reflect the basal rate of mRNA degradation, whereas co-treatment with TGF-β shows whether TGF-β enhances transcript decay.

Following treatment, total RNA was extracted and reverse-transcribed into cDNA. Transcript levels of *HSF2* and *Hsp70* were quantified using qRT-PCR, with *18S* rRNA serving as the internal reference for normalization. *Hsp70* mRNA, which is known to be highly stable and resistant to several decay pathways (Silver and Noble 2012), was included as a control to validate the experimental approach. Expression values were first normalized to *18S* and then to the 0-h baseline to allow fold-change comparisons. Fitted curves were generated using a

one-phase exponential decay model, excluding the 0 and 1-h data points due to the consistent transient peak observed in that window. Half-lives ($t_{1/2}$) were calculated from the fitted decay constants.

Upon ActD treatment, *HSF2* mRNA levels exhibited a transient increase, peaking at 1–2 h post-treatment. Despite this initial increase in mRNA levels, both *HSF2* and *Hsp70* transcript levels declined over the 8-h period (Figure 8). Comparison of the treatments indicated that *Hsp70* mRNA levels were lower in the presence of TGF-β, whereas *HSF2* mRNA levels were statistically unaffected by TGF-β treatment. These results indicate that the TGF-β-mediated suppression of HSF2 observed is attributable to transcriptional or post-translational mechanisms rather than accelerated mRNA decay.

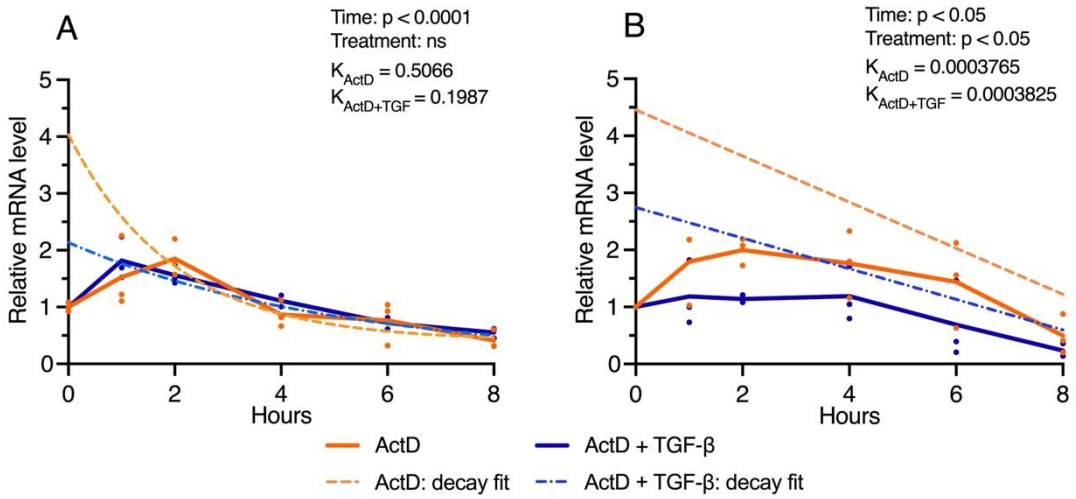

Figure 8. TGF-β's effect on *HSF2* and *Hsp70* mRNA stability in HS578T cells. (A) *HSF2* and (B) *Hsp70* mRNA levels were measured over 0–8 h in HS578T breast cancer cells treated with actinomycin D (ActD) ± TGF-β. Transcript levels were quantified by qRT-PCR, normalized to *18S* rRNA, and expressed relative to the 0 h timepoint. Data represent the mean of three independent measurements (n = 3). Decay curves were fitted using a one-phase exponential model applied to post-peak datapoints, excluding the 0–1 h window due to transient induction. Two-way ANOVA with time and treatment as factors revealed a significant time-dependent decrease in both *HSF2* ($p < 0.0001$) and *Hsp70* ($p < 0.05$). TGF-β affected *Hsp70* mRNA levels ($p < 0.05$) but had no effect on *HSF2*.

Calculation of transcript half-lives further supports this conclusion. *HSF2* mRNA displayed a half-life of 1.38 h under ActD treatment ($R^2 = 0.813$) and 3.49 h under ActD + TGF-β ($R^2 = 0.937$), suggesting that TGF-β may exert a modest protective effect on *HSF2* transcript stability. In contrast, decay modeling of *Hsp70* transcripts indicated relative stability, as reflected by low decay rates and long half-lives. *Hsp70* mRNA remained essentially stable under ActD alone ($t_{1/2}$ =1841 h; $R^2 = 0.485$) and under co-treatment with TGF-β ($t_{1/2}$ = 1812

h; $R^2 = 0.406$), an observation consistent with previous reports (Silver and Noble 2012). However, these low R^2 values (< 0.5) indicate that the exponential decay model did not adequately describe the *Hsp70* transcript levels. Therefore, while our results imply *Hsp70* transcript stability, the poor model fit lowers confidence in the half-time estimates, which are biologically implausible.

4.3 5'UTR is not the primary area responsible for TGF-β-induced *HSF2* promoter suppression

Having verified that TGF-β-mediated HSF2 downregulation occurs at the transcriptional level, we next sought to identify the promoter elements responsible for this effect. Because the full extent of the *HSF2* promoter has not yet been defined, a 2.5-kb sequence upstream of the *HSF2* gene was included in analyses to ensure the incorporation of potential distal regulatory elements, as sequences beyond 1.5 kb have not been investigated (Nykänen et al. 2001; Park et al. 2015). Earlier unpublished data from the Sistonen laboratory suggested that the TGF-β-responsive elements mediating HSF2 repression might reside within the proximal 5' untranslated region (UTR). However, the precise motifs involved in this repression remain unknown. To localize the putative elements mediating HSF2 downregulation, HS578T human breast cancer cells were transfected with a series of firefly luciferase reporter constructs in which luciferase expression was driven by either the full-length 5'UTR, one of four 5'UTR deletion variants, each lacking a distinct region of the sequence (designated ΔDel1–ΔDel4), or a promoter construct lacking the entire 5'UTR but retaining the upstream 1-kb region (1kbΔ5'UTR). An MMP9 reporter containing four SBEs was used as a positive control for TGF-β responsiveness.

Transfected cells were then treated with TGF-β or control medium, followed by measurement of luciferase and co-transfected β-galactosidase activities. Luciferase activity was quantified using a bioluminescence assay, in which the luciferase enzyme catalyzes the oxidation of its substrate, luciferin, in the presence of ATP, oxygen, and Mg^{2+}. This reaction emits light peaking at ~560 nm, with the intensity proportional to active luciferase levels, providing an indirect measure of promoter activity. To account for differences in transfection efficiency, cells were co-transfected with *lacZ* reporter plasmids driven by a constitutive promoter. The *lacZ* gene encodes β-galactosidase, which hydrolyses its ONPG substrate producing o-nitrophenol, a yellow chromophore measurable at 420 nm. Similarly, the absorbance intensity of the chromophore correlates with β-galactosidase activity. Luciferase values were first normalized to β-galactosidase, to control for transfection efficiency, and then, within each

biological replicate, to the corresponding untreated control, yielding fold-change values relative to baseline.

As expected, the MMP9 reporter was activated by TGF-β ($p < 0.05$), confirming treatment efficacy. Unexpectedly, the strongest TGF-β-induced repression of *HSF2* promoter activity was observed in the negative control construct 1kbΔ5'UTR (66.2 ± 2.4% reduction; $p < 0.0001$), rather than in the full 5'UTR or its deletion variants (Figure 9A). Among the deletion constructs, ΔDel2–4 showed moderate but significant TGF-β-induced repression (35–56%, all $p < 0.01$), whereas ΔDel1 (lacking the transcription start site, TSS) displayed high variability and no significant repression. This variability may reflect disruption of basal promoter activity caused by TSS removal. However, because 1kbΔ5'UTR, which also lacks the TSS, exhibited the strongest downregulation under TGF-β stimulation, the absence of TSS alone is unlikely to account for the observed effect. Together, these findings suggest that sequences upstream of the 5'UTR, rather than the 5'UTR itself, contain the major TGF-β-responsive elements.

To reconcile the inconsistent repression patterns observed in the 5'UTR deletion constructs, we next examined promoter fragments spanning broader regions of the *HSF2* promoter. The 0.5kb construct, containing the 5'UTR and its 0.5-kb upstream region, exhibited the strongest repression (82.4 ± 4.7%). Deletion of this 0.5-kb segment from the full-length promoter (2kbΔ0.5kb) reduced repression by more than two-fold (37.0 ± 14.4%) (Figure 9A). In comparison, the full-length 2.5-kb promoter and 1-kb promoter, both containing the 5'UTR and its flanking 0.5-kb region, exhibited intermediate repression with higher variability (58.4 ± 20% and 62.7 ± 17% respectively; $p < 0.05$). To directly evaluate the contribution of the 0.5-kb region, repression of the 2.5kb and 2kbΔ0.5kb constructs was compared. Although repression tended to be stronger in the intact 2.5-kb promoter (62.7% vs. 37.0%), the difference did not reach statistical significance (Welch's t-test, $p \approx 0.06$).

To further contextualize these observations, we next examined basal promoter activity using raw luciferase values normalized only to β-galactosidase (Figure 9B). Interestingly, ΔDel1 (which lacks the TSS) displayed highly variable yet elevated basal activity ($4.2 \times 10^5 \pm 2.0 \times 10^5$), even exceeding that of the isolated 5'UTR construct (2.4×10^5). This may reflect instability arising from TSS removal, leading to aberrant promoter activity. Constructs retaining both the 5'UTR and the upstream 0.5-kb region displayed ~20-fold higher basal activity ($\sim 2 \times 10^6$ RLU) than those lacking one or both elements ($\sim 1 \times 10^5$ RLU), indicating that these regions act cooperatively to sustain high promoter activity under basal conditions.

A direct comparison between the 2.5kb and 2kbΔ0.5kb constructs further highlighted this effect: basal activity of the 2.5-kb promoter was ~30-fold higher than that of 2kbΔ0.5kb (2.5×10^6 vs 8.2×10^4 RLU), and this difference was statistically significant (Welch's t-test, $p < 0.05$).

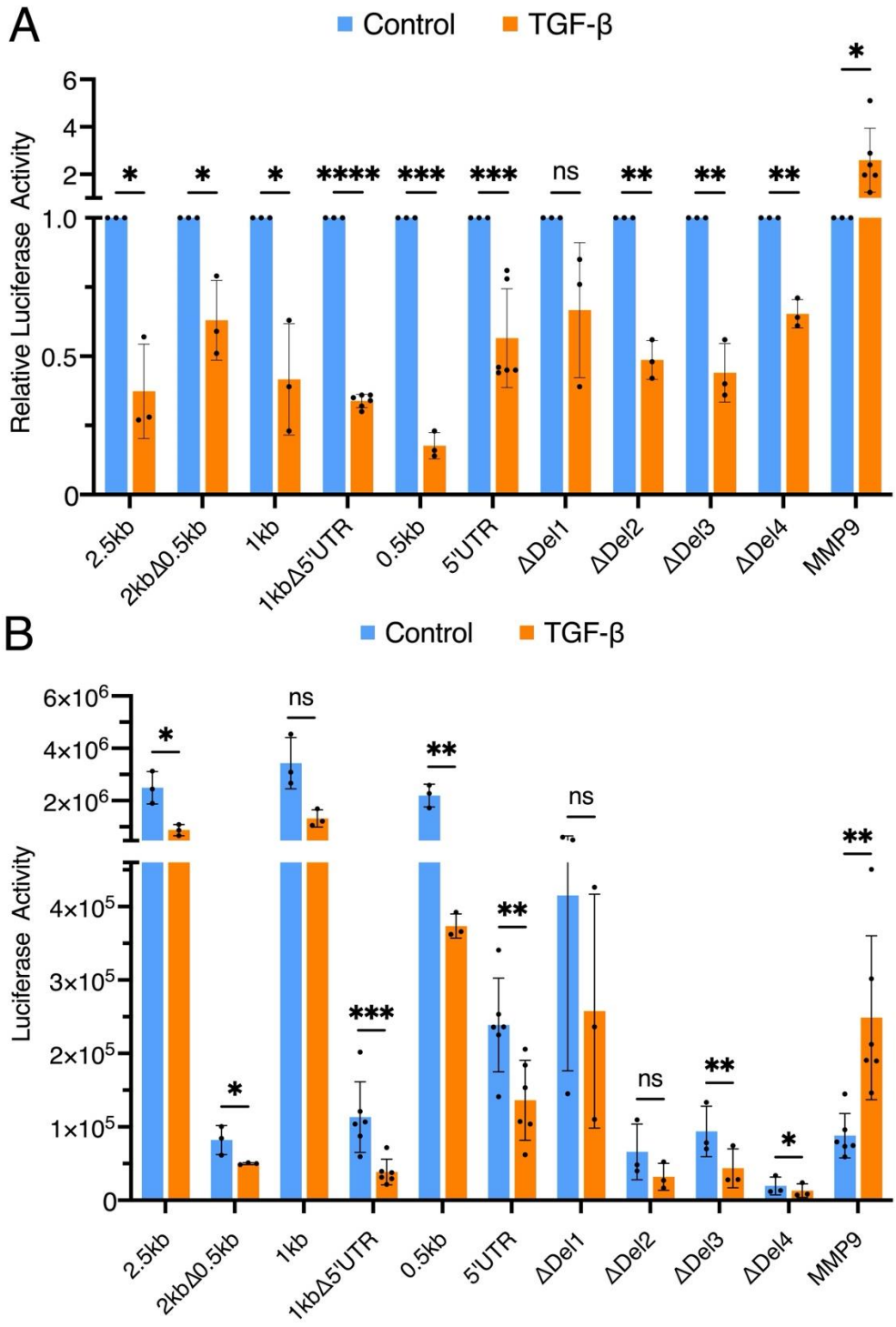

Figure 9. Luciferase reporter activity in HS578T cells following TGF-β stimulation. (A) Fold change in firefly luciferase activity relative to control. All constructs retaining a portion of the *HSF2* promoter, except ΔDel1, exhibited statistically significant repression. The strongest inhibition was observed in the 0.5-kb construct, with an 82.4 ± 4.7% reduction in activity. (B) Raw luciferase activity

values normalized to β-galactosidase, illustrating baseline transcriptional output across constructs. This panel provides context for absolute promoter strength independent of fold change normalization. As a positive control for TGF-β responsiveness, the MMP9 promoter construct displayed increased activity. After FDR correction, repression remained statistically significant for all constructs except 2kbΔ0.5kb. Data are presented as mean ± SD (n = 3 for all constructs; n = 6 for 1kbΔ5'UTR, 5'UTR, and MMP9). Statistical significance displayed in the figure is based on uncorrected p-values from: one-sample, one-tailed t-test against a hypothetical mean of 1 for fold-change data; paired one-tailed t-tests for raw luminescence values (TGF-β vs. control). ns: $p > 0.05$; *: $p < 0.05$; **: $p < 0.01$; ***: $p < 0.001$; ****: $p < 0.0001$.

Together, these findings demonstrate that the 5'UTR and its adjacent 0.5-kb upstream region are essential for maintaining high basal *HSF2* promoter activity, while the 0.5-kb segment, rather than the 5'UTR itself, contains the principal TGF-β-responsive elements mediating the HSF2 downregulation. While the difference in repression between constructs with and without this region did not reach statistical significance in the fold-change analysis, the pronounced loss of basal activity upon its deletion strongly implicates this segment as an important functional element within the *HSF2* promoter.

Although the statistical significance shown in Figure 9 is based on uncorrected p-values, the data were also evaluated using the Benjamini-Hochberg FDR correction (analysis not included in the thesis). After correction, only a single construct (2kbΔ0.5kb) lost significance in the raw luminescence analysis (Figure 9B); all other conclusions remained unchanged. This does not alter the overall interpretation but rather reinforces the conclusion that deletion of the upstream 0.5-kb region diminishes TGF-β-mediated repression, identifying this segment as the likely TGF-β-responsive element.

Across all *HSF2* promoter truncations tested, the results converged consistently: the 0.5-kb region immediately upstream of the 5'UTR contributed substantially to both basal promoter activity and TGF-β responsiveness. This contrasts with the earlier unpublished data suggesting that the 5'UTR would contain the primary TGF-β-responsive elements. Given the consistency of our results across multiple truncated *HSF2* promoter constructs, we conclude that the 0.5-kb upstream region represents the most plausible candidate for containing the putative TF binding sites through which TGF-β-mediated repression of HSF2 is likely to occur.

4.4 Detergent use and mechanical disruption are critical for resolving subcellular compartments of HS578T breast cancer cells

The DAP experiment was designed to isolate nuclear proteins capable of interacting with the *HSF2* promoter region identified in the luciferase assays as TGF-β-responsive. Because any regulatory factors acting on this promoter segment are expected to reside in the nucleus

following TGF-β stimulation, the first step required preparing nuclear extracts. To achieve this, HS578T cells treated with either control medium or TGF-β were subjected to subcellular fractionation, beginning with selective disruption of the plasma membrane to remove cytoplasmic proteins while preserving the nuclear envelope. As the goal of DAP is to capture proteins present in the nucleus following their TGF-β-induced nuclear accumulation, further separation of the chromatin fraction was not performed in all experiments. Several fractionation strategies were heuristically tested to enhance nuclear protein concentration and purity. These included a commercial kit, variations in buffer composition and DNA-digestion methods, and the use of mechanical disruption.

To evaluate the specificity of each protocol, samples were collected from whole cell lysate, cytoplasmic, nuclear, and debris fractions for immunoblotting with compartment markers (α-tubulin for cytoplasm, lamin A/C for nucleus, and histone H4 for chromatin). In some experiments, chromatin was isolated separately; however, for nuclear extract preparation, nuclear and chromatin fractions were ultimately combined. During later optimization, DNA digestion was performed concurrently with nuclear lysis by sonication, generating a single nuclear-chromatin fraction enriched in nuclear and DNA-associated proteins.

The commercial NE-PER™ kit (Thermo Fisher Scientific) reproducibly separated cellular compartments (Figure 10A) but was not adopted for routine use due to cost considerations. Among the non-commercial protocols, buffer composition proved critical: those lacking detergent produced poorly resolved fractions with substantial numbers of intact cells retained in the debris fraction (Figure 10B-C). Likewise, omitting Dounce homogenization resulted in inefficient lysis, evidenced by high levels of cytoplasmic markers (α-tubulin) in the debris fraction and excessively dilute nuclear extracts (Figure 10B). These challenges may reflect the properties of HS578T cells, which possess well-developed cytoskeletal networks that facilitate migration and invasion and may increase resistance to membrane disruption. The best results, based on nuclear extract concentration and acceptable purity, were obtained by combining a mild detergent with mechanical disruption by Dounce homogenization (Figure 10D). This procedure produced highly concentrated nuclear extracts that contained low levels of cytoplasmic protein. Sucrose supplementation further reduced extraction efficiency (Figure 10D). Although classically used to preserve nuclear morphology, sucrose stabilized the nuclear envelope to an extent that hindered nuclear lysis. Even in the presence of detergent, sucrose-containing buffers retained intact nuclei in the cytoplasmic fraction, leading to incomplete and inconsistent fractionation.

Across all non-commercial protocols, cytoplasmic fractions were highly dilute and required concentration prior to analysis. This concentration step inadvertently increased salt and detergent levels, promoting protein precipitation and reduced solubility. As a result, cytoplasmic fractions frequently produced weak or barely detectable marker signals, limiting their utility for assessing the efficacy and specificity of the initial plasma-membrane lysis.

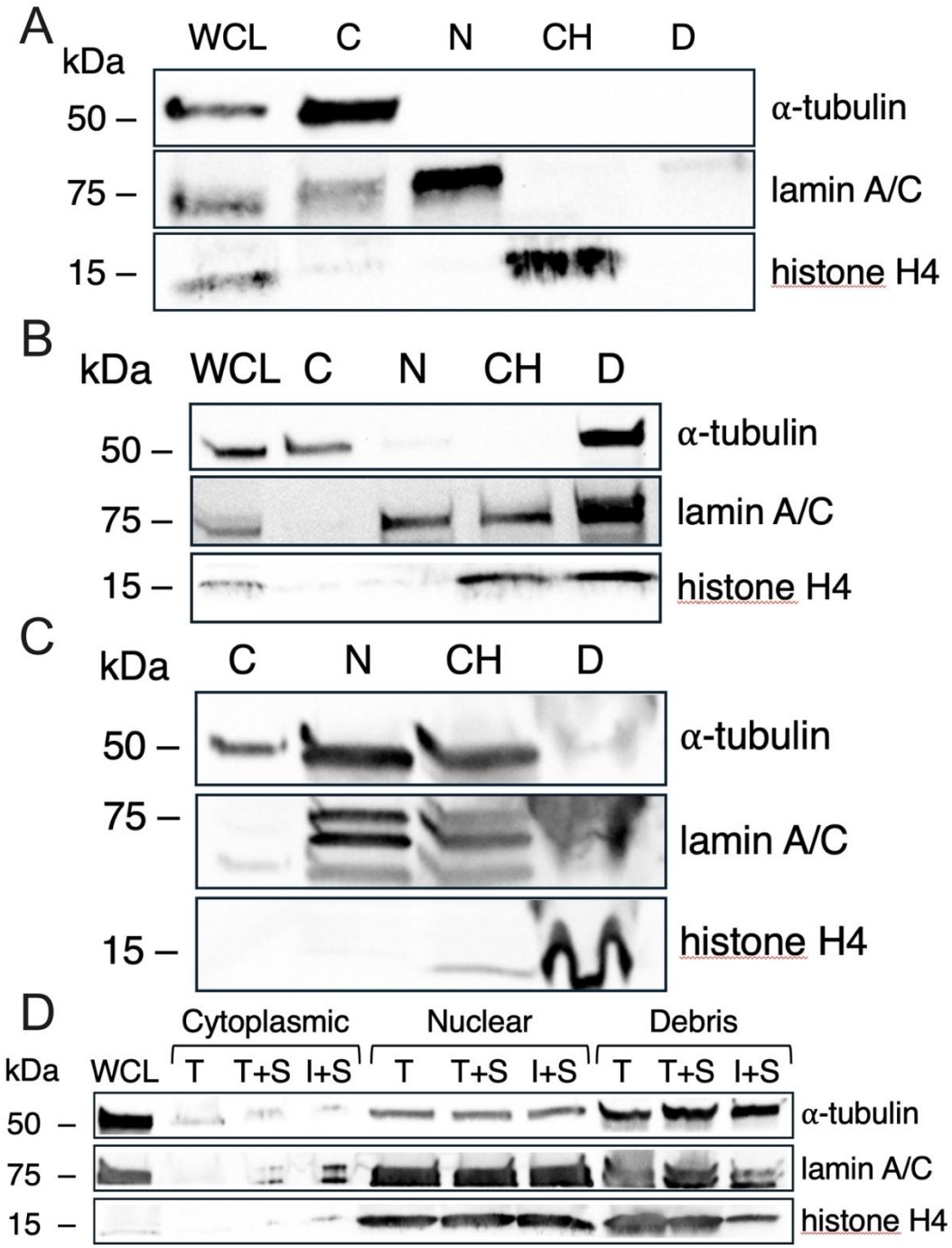

Figure 10. Immunoblot analysis of HS578T cells fractionated using different subcellular extraction methods for nuclear extract preparation. (A) Commercial NE-PER™ kit. (B) Nuclear extract preparation based on the DAP protocol modified from Müller and Engeland (2021). (C) Fractionation using Dounce homogenization based on Mahat et al. (2016). (D) Optimization combining

Dounce homogenization and sonication. Three extraction buffers were tested: Triton X-100 (T), Igepal (I), and the same buffers supplemented with 300 mM sucrose (T+S, I+S). Sucrose partially stabilized the nuclear envelope, reducing nuclear lysis and resulting in intact nuclei to contaminating cytoplasmic fractions. Fraction purity was assessed using α-tubulin (cytoplasm), lamin A/C (nucleus), and histone H4 (chromatin). WCL, whole-cell lysate; C, cytoplasmic; N, nuclear; CH, chromatin; D, debris.

4.5 Successful DNA probe generation of expected length

Biotinylated DNA probes corresponding to selected regions of the *HSF2* promoter were generated by PCR for use in the DAP workflow, which requires DNA fragments to capture promoter-binding proteins from nuclear extracts. Initially, 500-bp probes spanning the entire 2.5-kb *HSF2* promoter were designed. However, pilot affinity purifications revealed extensive non-specific protein binding, likely due to the high number of potential protein-DNA binding sites within long sequences. Because DAP is intended to isolate promoter-bound proteins of interest, limiting non-specific interactions is important. Therefore, a second set of shorter overlapping 144-bp probes covering the proximal 0.5-kb region of the *HSF2* promoter was generated. All probes were successfully amplified under optimized PCR conditions. Agarose gel electrophoresis confirmed clean single bands of the expected size. For every probe, a representative example is shown in Figure 11.

Figure 11. Size verification of biotinylated DNA probe amplification. A representative agarose gel showing successful amplification of a 144-bp 5'biotinylated *HSF2* promoter probe (probe 3), alongside a 100-bp Penn State DNA ladder. All seven probes produced identical single bands of expected size.

4.6 DNA affinity purification requires further optimization to improve specificity

To purify and identify TGF-β responsive TFs binding to the *HSF2* promoter, a DAP protocol was piloted. To reduce non-specific binding, DNA probes were blocked with sonicated salmon sperm DNA (100 or 200 μg/ml). Nuclear extracts from control- and TGF-β-treated

HS578T cells were pre-cleared and incubated with the probes, followed by pull-down using streptavidin-coated magnetic beads.

Whole-protein staining from the 500-bp probe pilot showed extensive protein binding across all probes, with TGF-β-treated samples retaining higher total protein levels compared to their control counterparts (Figure 12A). Immunoblotting further demonstrated that the eluates lacked sequence specific DNA-TF interactions: p-Smad2 was detected in all TGF-β-treated eluates regardless of whether the probe contained SBEs (Figure 12C). Likewise, HSF1 was detected not only on the pHSF1 probe but also on the negative and positive control probes, despite these lacking HSF1-binding motifs. Therefore, the initial DAP setup lacked the specificity needed for reliable TF identification.

To decrease non-specific protein retention observed with the 500-bp probes, a second pilot was performed using shorter 144-bp probes, combined with increased DNA blocking concentrations and bead pre-clearing. This modified protocol substantially reduced background protein binding compared with the long probes (Figure 12B). However, whole-protein staining revealed similar protein profiles across all probes and treatment conditions, indicating that sufficient probe-specific enrichment for downstream mass spectrometry analysis was still not achieved.

Because none of the tested probes yielded selective protein purification, the eluates did not meet the quality requirements for mass spectrometry. Further optimization potentially involving modified buffers, protocol steps or different affinity-based strategies will be required before TF identification via mass spectrometry can be pursued.

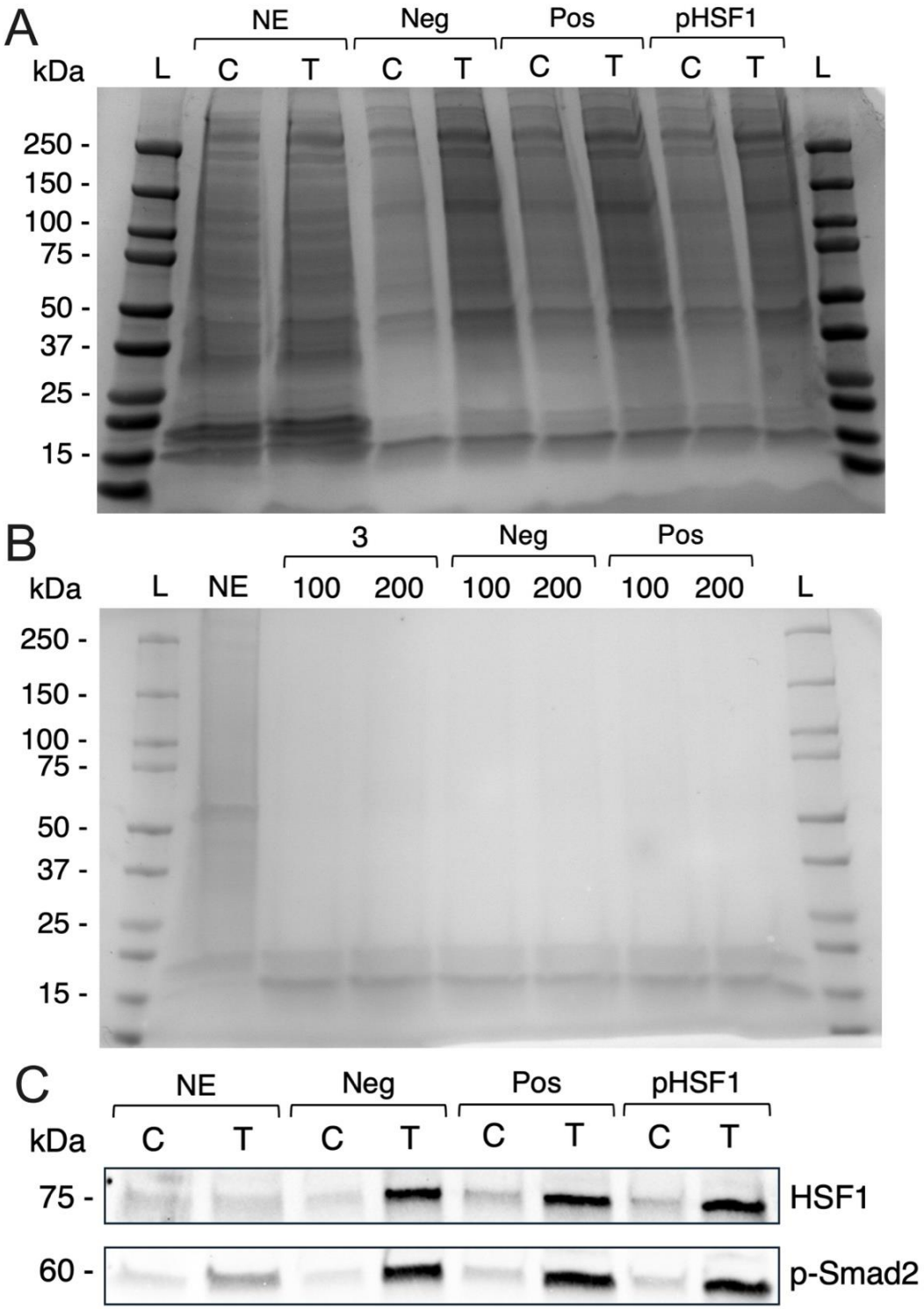

Figure 12. DNA affinity purification using 500-bp and 144-bp *HSF2* promoter probes. (A) Whole-protein staining of eluates from the 500-bp pilot shows extensive non-specific binding, with similar results across DNA probes incubated with nuclear extracts (NEs) from control (C) and TGF-β-treated (T) HS578T cells. TGF-β-treated samples consistently show higher overall protein retention. (B) Whole-protein staining from DAP using 144-bp probes incubated with TGF-β-treated NEs demonstrates reduced background relative to the 500-bp probe pilot, but no probe-, or treatment-specific enrichment. Blocking DNA concentration (100 vs 200 µg/ml) also produced no detectable differences. (C) Immunoblot from the 500-bp pilot showing HSF1 and p-Smad2 detected across all TGF-β-treated samples. L = ladder; NE = nuclear extract; Neg = negative control DNA probe; Pos = positive control DNA probe; pHSF1 = probe containing an HSF1-binding site; HSF1 = heat shock factor 1; p-Smad2 = phosphorylated Smad2.

5 Discussion and conclusions

TGF-β signaling is a potent driver of EMT and cancer cell invasion. Recently, Pessa and coworkers (2025) identified that TGF-β suppresses HSF2 expression in breast cancer cells during EMT, linking HSF2 downregulation to the acquisition of invasive properties. Since this suppression appears to participate in the early steps of the metastatic cascade, understanding how TGF-β represses HSF2 is biologically relevant. This thesis aimed to examine the mechanism underlying this repression and to identify the promoter regions and TFs mediating this response. Whether this repression occurs on a transcriptional level has not been previously investigated in detail. Here we show that the repression is either transcriptional or post-translational, as TGF-β does not promote *HSF2* transcript degradation in HS578T cells, indicating that the downregulation cannot be attributed to mRNA decay. Luciferase reporter assays revealed that the major TGF-β-responsive region lies within a 0.5-kb promoter segment upstream of the 5'UTR, rather than within the 5'UTR itself. Finally, although DAP was theoretically promising for identifying TGF-β-responsive TFs, the method lacked specificity under the tested conditions, revealing methodological limitations that must be resolved before continuing to mass spectrometry-based identification.

5.1 Interplay of TGF-β-mediated repression and early stress responses in actinomycin D chase experiment

A prerequisite for this study was to determine whether TGF-β suppresses HSF2 by promoting its transcript degradation. The ActD chase experiment demonstrated that *HSF2* transcript stability remains unchanged under TGF-β treatment, firmly indicating that repression is not mediated by mRNA decay. However, the early kinetics of ActD treatment were unusual: both *HSF2* and *Hsp70* mRNA levels transiently increased during the first hours. This behavior could have two explanations. First, ActD does not immediately halt elongating polymerases, resulting in a transient accumulation of transcripts before transcription fully ceases. Second, ActD is strongly cytotoxic and induces robust cellular stress responses (Sawicki and Godman 1971), which can transiently activate stress-responsive genes. A similar early induction of *Hsp70* under ActD was reported by Mivechi and coworkers (1992) – although in a different experimental context involving heat shock – supporting the interpretation that the observed transient peaks result from overlapping delayed transcriptional arrest and stress-induced transcription.

Canonical Smad signaling is the best-characterized pathway for TGF-β-mediated transcriptional regulation and has been implicated in HSF2 suppression (Pessa et al. 2025). Although TGF-β also activates several non-canonical pathways, whose contributions cannot yet be excluded, the kinetics of the canonical pathway provide a useful reference point. Because canonical TGF-β signaling undergoes rapid activation, where phosphorylated Smad2 becomes detectable within minutes (Zi et al. 2011), one might expect TGF-β-mediated HSF2 repression to manifest early in the TGF-β + ActD co-treatment. Instead, early *HSF2* mRNA levels increased and resembled those observed with ActD alone, suggesting that acute stress responses induced by ActD may obscure TGF-β-dependent transcriptional repression at early timepoints. Importantly, this study assessed HSF2 expression primarily at 8 h and 24 h after TGF-β exposure, and the recent findings by Pessa and coworkers (2025) similarly reported repression at 24 h. Thus, while the suppression at these later stages is well supported, the precise onset of HSF2 downregulation remains unknown. Determining how rapidly HSF2 is repressed following TGF-β stimulation would aid in interpreting the early decay-phase behavior in the ActD chase experiment. If HSF2 repression occurs within the first 1–4 h, ActD-induced stress responses may be masking it, whereas if repression occurs later, the early-phase kinetics observed here would be consistent with delayed transcriptional effects. This uncertainty reveals the need for more timepoints in future experiments to precisely define when TGF-β-mediated HSF2 repression begins.

Because HSF2 responds to stress in a context-dependent manner, ActD-induced cytotoxicity may transiently activate HSF2 transcription. The well-established stress-inducible chaperone Hsp70 provides a useful parallel: ActD alone elicited a strong induction, whereas the co-treatment with TGF-β dampened the response to small oscillations. This suggests that TGF-β may interfere with the ActD stress-induced transcription. As a result, the early phase of the assay is characterized by stress-induced transcription rather than decay kinetics, and only after this transient window do decay dynamics become interpretable. Nonetheless, our data clearly indicate that TGF-β does not decrease *HSF2* mRNA half-life, reinforcing the conclusion that the observed HSF2 suppression is driven primarily by transcriptional or post-transcriptional regulation.

5.2 A promoter-proximal 0.5-kb region mediates TGF-β-responsive repression of HSF2

Luciferase reporter assays provided new insight into the location of the promoter region responsible for TGF-β-mediated repression of HSF2, the mechanistic details of which has

remained uncharacterized. Earlier unpublished observations had suggested that these promoter elements were located within the 5'UTR. However, across two complementary sets of promoter truncations, our results consistently identified a 0.5-kb segment immediately upstream of the 5'UTR as the major TGF-β-responsive element. Constructs containing this 0.5-kb segment showed the most prominent TGF-β-induced repression, whereas deletion of this region significantly weakened suppression and reduced basal promoter activity. Although the 5'UTR itself did not emerge as the primary area of interest, constructs containing both the 5'UTR and the adjacent upstream region displayed the highest basal activity, suggesting that these two regions cooperate to sustain strong transcription under basal conditions.

Interestingly, nearly all constructs retaining any portion of the *HSF2* promoter still exhibited significant repression in response to TGF-β, despite extensive internal deletions. This suggests that the *HSF2* promoter contains a distributed and potentially redundant network of regulatory elements, where multiple motifs mediating activating and repressive signals contribute collectively to transcriptional modulation. Such combinatorial regulation aligns with the nature of TGF-β signaling, which often integrates signals from multiple TFs downstream of canonical and non-canonical pathways (Massagué and Sheppard 2023). Within this framework, the 0.5-kb upstream region emerged as a central TGF-β-responsive segment and represents a strong candidate for future motif mapping and TF-binding and -identifying studies.

5.3 Technical limitations of DAP and challenges in TF pull-down

The DAP experiments were intended to identify TFs binding to these regions, but the approach proved technically limited under the tested conditions. As expected, nuclear p-Smad2 levels increased following TGF-β treatment. However, p-Smad2 was pulled-down from all the nuclear extracts derived from TGF-β-treated cells, regardless of whether the DNA probes contained SBEs. A similar pattern was observed for HSF1, which was also pulled-down from all TGF-β-treated samples even when the DNA probes lacked its binding motifs. Because HSF1 levels are not influenced by TGF-β signaling (Pessa et al. 2025), its selective enrichment only in TGF-β-treated samples is unexpected. These observations mirror the whole-protein staining results, where TGF-β-treated samples consistently displayed higher overall protein retention compared to their control counterparts, despite equal input amounts. Together, these findings suggest that the current DAP setup favored non-specific retention of proteins in TGF-β-treated samples, rather than specific motif-dependent binding. It remains

unclear whether the limiting factor was insufficient blocking, properties intrinsic to HS578T nuclear extracts, probe design, buffer composition, or a broader limitation associated with the DAP protocol. Because the eluates lacked specificity, they were unsuitable for mass spectrometry, and substantial methodological optimization will be required before reliable TF identification can be achieved.

5.4 Methodological and biological limitations of the study

This study has several limitations that should be considered when interpreting the findings. Only a single breast cancer cell line, the triple-negative and inherently invasive HS578T (Conner et al. 2024), was examined. Whether the same regulatory logic applies in non-invasive or primary breast epithelial cells remains unknown, and the use of a cell line already exhibiting invasive behavior may obscure earlier regulatory events.

The cytotoxicity associated with ActD may affect stress-responsive transcriptional programs, including those of the HSF family, and therefore may not be the most suitable approach for assessing mRNA degradation in this context. A more appropriate alternative would be to measure nascent RNA using metabolic-labeling approaches, which allow quantification of newly synthesized transcripts without inducing strong cellular stress responses. Use of labels such as the nucleotide-analog 4-thiouridine offers a more accurate means to assess transcriptional activity and mRNA degradation under TGF-β treatment without the cytotoxic effects (Garibaldi et al. 2017).

Variability in β-galactosidase activity used in normalization complicates the interpretation of the effect of promoter inserts on firefly luciferase activity. The variability may arise from the fact that β-galactosidase quantification required cell harvesting and lysis, whereas luciferase was measured directly from live cells in-well, leading to additional technical variability between the two assays. In future experiments, a normalization strategy assayed under identical conditions to firefly luciferase would be preferable. For example, utilization of a dual-luciferase system, in which a constitutively expressed Renilla luciferase is co-transfected and quantified from the same sample, would minimize technical variation and provide a more reliable internal control. Additionally, including an empty luciferase vector lacking promoter inserts would help verify that basal background luminescence is minimal.

5.5 Conclusions and future directions

In conclusion, this study demonstrates that TGF-β suppresses HSF2 expression through transcriptional mechanisms rather than mRNA degradation, and it identifies a 0.5-kb upstream promoter region as the principal TGF-β-responsive segment mediating this downregulation. Although the TFs mediating this repression could not be identified due to methodological limitations in the DAP protocol, the defined promoter region provides a focused starting point for future studies. In particular, the 0.5-kb region could be targeted in chromatin immunoprecipitation assays to test for binding by canonical Smad partners, e.g. Snail and Zeb1. Understanding the mechanistic basis of TGF-β-mediated repression of HSF2 is important because in breast cancer HSF2 downregulation promotes the acquisition of invasive traits associated with EMT (Pessa et al. 2025). Since forced HSF2 expression counteracts this shift towards an invasive phenotype, the mechanism underlying HSF2 downregulation represents a candidate signaling axis for therapeutic targeting. To clarify how HSF2 downregulation contributes to the invasive phenotypic switch in breast cancer progression, it will be necessary to identify the TGF-β-responsive transcriptional repressors that interact with the promoter-proximal 0.5-kb region, determine how TGF-β signaling modulates their activity, and establish how these factors alter promoter function. Such mechanistic insight could enable the discovery and development of targeted therapies to interfere with the invasive switch and curb metastatic dissemination, the leading cause of cancer-related mortality.

References

Abane, R. & Mezger, V. (2010) Roles of heat shock factors in gametogenesis and development. *FEBS J* **277**:4150–4172.

Ahlskog, J. K., Björk, J. K., Elsing, A. N., Aspelin, C., Kallio, M., Roos-Mattjus, P. & Sistonen, L. (2010) Anaphase-promoting complex/cyclosome participates in the acute response to protein-damaging stress. *Molecular and Cellular Biology* **30**:5608–5620.

Akimov, V., Barrio-Hernandez, I., Hansen, S. V. F., Hallenborg, P., Pedersen, A.-K., Bekker-Jensen, D. B., …, & Blagoev, B. (2018) UbiSite approach for comprehensive mapping of lysine and N-terminal ubiquitination sites. *Nat Struct Mol Biol* **25**:631–640.

Amin, J., Ananthan, J. & Voellmy, R. (1988) Key features of heat shock regulatory elements. *Mol Cell Biol* **8**:3761–3769.

Annes, J. P., Rifkin, D. B. & Munger, J. S. (2002) The integrin α_V β_6 binds and activates latent TGFβ3. *FEBS Lett* **511**:65–68.

Aprile-Garcia, F., Tomar, P., Hummel, B., Khavaran, A. & Sawarkar, R. (2019) Nascent-protein ubiquitination is required for heat shock–induced gene downregulation in human cells. *Nat Struct Mol Biol* **26**:137–146.

Bartolomucci, A., Nobrega, M., Ferrier, T., Dickinson, K., Kaorey, N., Nadeau, A., …, & Burnier, J. V. (2025) Circulating tumor DNA to monitor treatment response in solid tumors and advance precision oncology. *NPJ Precis Oncol* **9**:84.

Bierie, B. & Moses, H. L. (2006) TGFβ: the molecular Jekyll and Hyde of cancer. *Nat Rev Cancer* **6**:506–520.

Bilandzic, M. & Stenvers, K. L. (2011) Betaglycan: a multifunctional accessory. *Mol Cell Endocrinol* **339**:180–189.

Björk, J. K., Åkerfelt, M., Joutsen, J., Puustinen, M. C., Cheng, F., Sistonen, L. & Nees, M. (2016) Heat-shock factor 2 is a suppressor of prostate cancer invasion. *Oncogene* **35**:1770–1784.

Björk, J. K., Sandqvist, A., Elsing, A. N., Kotaja, N. & Sistonen, L. (2010) miR-18, a member of Oncomir-1, targets heat shock transcription factor 2 in spermatogenesis. *Development* **137**:3177–3184.

Björk, J. K. & Sistonen, L. (2010) Regulation of the members of the mammalian heat shock factor family. *FEBS J* **277**:4126–4139.

Brabletz, S., Schuhwerk, H., Brabletz, T. & Stemmler, M. P. (2021) Dynamic EMT: a multi-tool for tumor progression. *EMBO J* **40**:e108647.

Bracken, C. P., Gregory, P. A., Kolesnikoff, N., Bert, A. G., Wang, J., Shannon, M. F. & Goodall, G. J. (2008) A double-negative feedback loop between ZEB1-SIP1 and the microRNA-200 family regulates epithelial-mesenchymal transition. *Cancer Res* **68**:7846–7854.

Calderwood, S. K. (2012) Elevated levels of HSF1 indicate a poor prognosis in breast cancer. *Future Oncol*. **8:**399–401

Cao, Z.-Q., Wang, Z. & Leng, P. (2019) Aberrant N-cadherin expression in cancer. *Biomed Pharmacother* **118**:109320.

Capocci, M., Santoro, M. G. & Hightower, L. E. (2014) The life and times of Ferruccio Ritossa. *Cell Stress Chaperones* **19**:599–604.

Carvalho-cruz, P., Alisson-Silva, F., Todeschini, A. R. & Dias, W. B. (2018) Cellular glycosylation senses metabolic changes and modulates cell plasticity during epithelial to mesenchymal transition. *Dev Dyn* **247**:481–491.

Chan, K., Fu, S., Wong, Y., Hui, W., Cheuk, Y. & Wong, M. W. (2008) Expression of transforming growth factor β isoforms and their roles in tendon healing. *Wound Repair Regen* **16**:399–407.

Choi, H., Park, J., Park, M., Won, H., Joo, H., Lee, C. H., …, & Kong, G. (2015) UTX inhibits EMT-induced breast CSC properties by epigenetic repression of EMT genes in cooperation with LSD1 and HDAC1. *EMBO Rep* **16**:1288–1298.

Conner, S. J., Guarin, J. R., Le, T. T., Fatherree, J. P., Kelley, C., Payne, S. L., …, & Oudin, M. J. (2024) Cell morphology best predicts tumorigenicity and metastasis in vivo across multiple TNBC cell lines of different metastatic potential. *Breast Cancer Res BCR* **26**:43.

Dai, C., Dai, S. & Cao, J. (2012) Proteotoxic stress of cancer: implication of the heat-shock response in oncogenesis. *J Cell Physiol* **227**:2982–2987.

Dai, C., Whitesell, L., Rogers, A. B. & Lindquist, S. (2007) Heat shock factor 1 is a powerful multifaceted modifier of carcinogenesis. *Cell* **130**:1005–1018.

Dai, S., Tang, Z., Cao, J., Zhou, W., Li, H., Sampson, S. & Dai, C. (2015) Suppression of the HSF1-mediated proteotoxic stress response by the metabolic stress sensor AMPK. *EMBO J* **34**:275–293.

Daupin, K., Dubreuil, V., Ahlskog, J. K., Verrico, A., Sistonen, L., Mezger, V. & De Thonel, A. (2025) HDAC1 is involved in the destabilization of the HSF2 protein under nonstress and stress conditions. *Cell Stress and Chaperones* **30**:100079.

David, C. J., Huang, Y.-H., Chen, M., Su, J., Zou, Y., Bardeesy, N., …, & Massagué, J. (2016) TGF-β tumor suppression through a lethal EMT. *Cell* **164**:1015–1030.

de Almeida, L. G. N., Thode, H., Eslambolchi, Y., Chopra, S., Young, D., Gill, S., …, & Dufour, A. (2022) Matrix metalloproteinases: from molecular mechanisms to physiology, pathophysiology, and pharmacology. *Pharmacol Rev* **74**:714–770.

De Blander, H., Tonon, L., Fauvet, F., Pommier, R. M., Lamblot, C., Benhassoun, R., …, & Puisieux, A. (2024) Cooperative pro-tumorigenic adaptation to oncogenic RAS through epithelial-to-mesenchymal plasticity. *Sci Adv* **10**:eadi1736.

De Thonel, A., Ahlskog, J. K., Daupin, K., Dubreuil, V., Berthelet, J., Chaput, C., …, & Mezger, V. (2022) CBP-HSF2 structural and functional interplay in Rubinstein-Taybi neurodevelopmental disorder. *Nat Commun* **13**:7002.

Debnath, P., Huirem, R. S., Dutta, P. & Palchaudhuri, S. (2021) Epithelial–mesenchymal transition and its transcription factors. *Biosci Rep* **42**:BSR20211754.

Deng, Z., Fan, T., Xiao, C., Tian, H., Zheng, Y., Li, C. & He, J. (2024) TGF-β signaling in health, disease and therapeutics. *Signal Transduct Target Ther* **9(1)**:61.

Derynck, R., Jarrett, J. A., Chen, E. Y., Eaton, D. H., Bell, J. R., Assoian, R. K., …, & Goeddel, D. V. (1985) Human transforming growth factor-β complementary DNA sequence and expression in normal and transformed cells. *Nature* **316**:701–705.

Desai, S., Liu, Z., Fodstad, O. & Tan, M. (2012) Abstract LB-488: induction of autophagy by heat shock factor 1 promotes breast cancer resistance to chemotherapy. *Cancer Res* **72**:LB-488-LB-488.

Di Gregorio, J., Robuffo, I., Spalletta, S., Giambuzzi, G., De Iuliis, V., Toniato, E., …, & Flati, V. (2020) The epithelial-to-mesenchymal transition as a possible therapeutic target in fibrotic disorders. *Front Cell Dev Biol* **8**:607483.

Dillekås, H., Rogers, M. S. & Straume, O. (2019) Are 90% of deaths from cancer caused by metastases? *Cancer Med* **8**:5574–5576.

Dongre, A. & Weinberg, R. A. (2019) New insights into the mechanisms of epithelial–mesenchymal transition and implications for cancer. *Nat Rev Mol Cell Biol* **20**:69–84.

Dubois, C. M., Laprise, M.-H., Blanchette, F., Gentry, L. E. & Leduc, R. (1995) Processing of Transforming growth factor β1 precursor by human furin convertase. *J Biol Chem* **270**:10618–10624.

Erinjeri, A. P., Wang, X., Williams, R., Chiozzi, R. Z., Thalassinos, K. & Labbadia, J. (2024) HSF-1 promotes longevity through ubiquilin-1-dependent mitochondrial network remodelling. *Nat Commun* **15**:9797.

Feng, H., Liu, W. & Wang, D.-C. (2016) Purification, crystallization and X-ray diffraction analysis of the DNA-binding domain of human heat-shock factor 2. *Acta Crystallogr Sect F Struct Biol Commun* **72**:294–299.

Feng, Z., Zi, Z. & Liu, X. (2016) Measuring TGF-β Ligand Dynamics in Culture Medium. *Methods Mol Biol* **1344**:379–389.

Fink, E. E., Zhang, Y., Santo, B., Siddavatam, A., Ou, R., Nanavaty, V., …, & Ting, A. H. (2025) Heat shock induces alternative polyadenylation through dynamic DNA methylation and chromatin looping. *Cell Stress Chaperones* **30**:100084.

Fiorenza, M. T., Farkas, T., Dissing, M., Kolding, D. & Zimarino, V. (1995) Complex expression of murine heat shock transcription factors. *Nucleic Acids Res* **23**:467–474.

Galle, E., Thienpont, B., Cappuyns, S., Venken, T., Busschaert, P., Van Haele, M., …, & Lambrechts, D. (2020) DNA methylation-driven EMT is a common mechanism of resistance to various therapeutic agents in cancer. *Clin Epigenetics* **12**:27.

Garibaldi, A., Carranza, F. & Hertel, K. J. (2017) Isolation of Newly Transcribed RNA Using the Metabolic Label 4-Thiouridine. In Y. Shi (Ed.), *mRNA Processing* (Vol. 1648, pp. 169–176). New York, NY: Springer.

Giarratana, A. O., Prendergast, C. M., Salvatore, M. M. & Capaccione, K. M. (2024) TGF-β signaling: critical nexus of fibrogenesis and cancer. *J Transl Med* **22**:594.

Gidalevitz, T., Prahlad, V. & Morimoto, R. I. (2011) The stress of protein misfolding: from single cells to multicellular organisms. *Cold Spring Harb Perspect Biol* **3**:a009704–a009704.

Gomez-Pastor, R., Burchfiel, E. T. & Thiele, D. J. (2018) Regulation of heat shock transcription factors and their roles in physiology and disease. *Nat Rev Mol Cell Biol* **19**:4–19.

Goodson, M. L., Park-Sarge, O.-K. & Sarge, K. D. (1995) Tissue-dependent expression of heat shock factor 2 isoforms with distinct transcriptional activities. *Mol Cell Biol* **15**:5288–5293.

Greenburg, G. & Hay, E. D. (1982) Epithelia suspended in collagen gels can lose polarity and express characteristics of migrating mesenchymal cells. *J Cell Biol* **95**:333–339.

Gregory, P. A., Bert, A. G., Paterson, E. L., Barry, S. C., Tsykin, A., Farshid, G., …, & Goodall, G. J. (2008) The miR-200 family and miR-205 regulate epithelial to mesenchymal transition by targeting ZEB1 and SIP1. *Nat Cell Biol* **10**:593–601.

Guettouche, T., Boellmann, F., Lane, W. S. & Voellmy, R. (2005) Analysis of phosphorylation of human heat shock factor 1 in cells experiencing a stress. *BMC Biochem* **6**:4.

Guo, L., Zhang, Y., Zhang, L., Huang, F., Li, J. & Wang, S. (2015) MicroRNAs, TGF-β signaling, and the inflammatory microenvironment in cancer. *Tumour Biol* **37**:115–125.

Hahn, J.-S. & Thiele, D. J. (2004) Activation of the *Saccharomyces cerevisiae* heat shock transcription factor under glucose starvation conditions by Snf1 protein kinase*. *J Biol Chem* **279**:5169–5176.

Hata, A. & Chen, Y.-G. (2016) TGF-β Signaling from Receptors to Smads. *Cold Spring Harb Perspect Biol* **8**:a022061.

He, L. & Hannon, G. J. (2004) MicroRNAs: small RNAs with a big role in gene regulation. *Nat Rev Genet* **5**:522–531.

Hill, L., Browne, G. & Tulchinsky, E. (2013) ZEB/miR-200 feedback loop: At the crossroads of signal transduction in cancer. *International Journal of Cancer* **132**:745–754.

Himanen, S. V., Puustinen, M. C., Da Silva, A. J., Vihervaara, A. & Sistonen, L. (2022) HSFs drive transcription of distinct genes and enhancers during oxidative stress and heat shock. *Nucleic Acids Research* **50**:6102–6115.

Huang, F. & Chen, Y.-G. (2012) Regulation of TGF-β receptor activity. *Cell Biosci* **2**:9.

Huber, M. A., Kraut, N. & Beug, H. (2005) Molecular requirements for epithelial–mesenchymal transition during tumor progression. *Curr Opin Cell Biol* **17**:548–558.

Hästbacka, H. S. E., Da Silva, A. J., Sistonen, L. & Henriksson, E. (2025) A guide to heat shock factors as multifunctional transcriptional regulators. *FEBS J* **292(16)**:4133–4155.

Ikushima, H. & Miyazono, K. (2010) TGFβ signalling: a complex web in cancer progression. *Nat Rev Cancer* **10**:415–424.

Jacobs, C., Shah, S., Lu, W.-C., Ray, H., Wang, J., Hockaden, N., …, & Carpenter, R. L. (2024) HSF1 Inhibits Antitumor Immune Activity in Breast Cancer by Suppressing CCL5 to Block CD8+ T-cell Recruitment. *Cancer Research* **84**:276–290.

Jaeger, A. M., Pemble, C. W., Sistonen, L. & Thiele, D. J. (2016) Structures of HSF2 reveal mechanisms for differential regulation of human heat-shock factors. *Nat Struct Mol Biol* **23**:147–154.

Jalali, A., Zhu, X., Liu, C. & Nawshad, A. (2012) Induction of palate epithelial mesenchymal transition by transforming growth factor β3 signaling. *Dev Growth Differ* **54**:633–648.

Javelaud, D. & Mauviel, A. (2005) Crosstalk mechanisms between the mitogen-activated protein kinase pathways and Smad signaling downstream of TGF-β: implications for carcinogenesis. *Oncogene* **24**:5742–5750.

Ji, Q., Li, H., Cai, Z., Yuan, X., Pu, X., Huang, Y., …, & Li, R. (2023) PYGL-mediated glucose metabolism reprogramming promotes EMT phenotype and metastasis of pancreatic cancer. *Int J Biol Sci* **19**:1894–1909.

Jin, X., Moskophidis, D. & Mivechi, N. F. (2011) Heat shock transcription factor 1 is a key determinant of HCC development by regulating hepatic steatosis and metabolic syndrome. *Cell Metab* **14**:91–103.

Joutsen, J., Da Silva, A. J., Luoto, J. C., Budzynski, M. A., Nylund, A. S., De Thonel, A., …, & Sistonen, L. (2020) Heat Shock Factor 2 Protects against Proteotoxicity by Maintaining Cell-Cell Adhesion. *Cell Reports* **30**:583-597.e6.

Joutsen, J., Pessa, J. C., Jokelainen, O., Sironen, R., Hartikainen, J. M. & Sistonen, L. (2024) Comprehensive analysis of human tissues reveals unique expression and localization patterns of HSF1 and HSF2. *Cell Stress Chaperones* **29**:235–271.

Joutsen, J. & Sistonen, L. (2019) Tailoring of proteostasis networks with heat shock factors. *Cold Spring Harb Perspect Biol* **11**:a034066.

Jullien, P., Berg, T. M. & Lawrence, D. A. (1989) Acidic cellular environments: activation of latent TGF-β and sensitization of cellular responses to TGF-β and egf. *Int J Cancer* **43**:886–891.

Kallio, M. (2002) Brain abnormalities, defective meiotic chromosome synapsis and female subfertility in HSF2 null mice. *EMBO J* **21**:2591–2601.

Kalluri, R. & Weinberg, R. A. (2009) The basics of epithelial-mesenchymal transition. *J Clin Invest* **119**:1420–1428.

Katsuno, Y., Lamouille, S. & Derynck, R. (2013) TGF-β signaling and epithelial–mesenchymal transition in cancer progression. *Curr Opin Oncol* **25**:76.

Kawazoe, Y., Nakai, A., Tanabe, M. & Nagata, K. (1998) Proteasome inhibition leads to the activation of all members of the heat-shock-factor family. *Eur J Biochem* **255**:356–362.

Kennecke, H., Yerushalmi, R., Woods, R., Cheang, M. C. U., Voduc, D., Speers, C. H., …, & Gelmon, K. (2010) Metastatic behavior of breast cancer subtypes. *J Clin Oncol* **28**:3271–3277.

Kim, E., Wang, B., Sastry, N., Masliah, E., Nelson, P. T., Cai, H. & Liao, F.-F. (2016) NEDD4-mediated HSF1 degradation underlies α-synucleinopathy. *Hum Mol Genet* **25**:211–222.

Kim, J., Harper, A., McCormack, V., Sung, H., Houssami, N., Morgan, E., …, & Fidler-Benaoudia, M. M. (2025) Global patterns and trends in breast cancer incidence and mortality across 185 countries. *Nat Med* **31**:1154–1162.

Kmiecik, S. W. & Mayer, M. P. (2022) Molecular mechanisms of heat shock factor 1 regulation. *Trends Biochem Sci* **47**:218–234.

Koch, A. W., Pokutta, S., Lustig, A. & Engel, J. (1997) Calcium binding and homoassociation of E-cadherin domains. *Biochemistry* **36**:7697–7705.

Korpal, M., Ell, B. J., Buffa, F. M., Ibrahim, T., Blanco, M. A., Celià-Terrassa, T., …, & Kang, Y. (2011) Direct targeting of Sec23a by miR-200s influences cancer cell secretome and promotes metastatic colonization. *Nat Med* **17**:1101–1108.

Kuo, W., Odenwald, M. A., Turner, J. R. & Zuo, L. (2022) Tight junction proteins occludin and ZO-1 as regulators of epithelial proliferation and survival. *Ann N Y Acad Sci* **1514**:21–33.

Lai, W. S., Arvola, R. M., Goldstrohm, A. C. & Blackshear, P. J. (2019) Inhibiting transcription in cultured metazoan cells with actinomycin D to monitor mRNA turnover. *Methods San Diego Calif* **155**:77–87.

Lamouille, S., Connolly, E., Smyth, J. W., Akhurst, R. J. & Derynck, R. (2012) TGF-β-induced activation of mTOR complex 2 drives epithelial–mesenchymal transition and cell invasion. *J Cell Sci* **125**:1259–1273.

Lamouille, S., Xu, J. & Derynck, R. (2014) Molecular mechanisms of epithelial–mesenchymal transition. *Nat Rev Mol Cell Biol* **15**:178–196.

Lee, J. H. & Massagué, J. (2022) TGF-β in developmental and fibrogenic EMTs. *Semin Cancer Biol* **86**:136–145.

Lee, J. H., Sánchez-Rivera, F. J., He, L., Basnet, H., Chen, F. X., Spina, E., …, & Massagué, J. (2024) TGF-β and RAS jointly unmask primed enhancers to drive metastasis. *Cell* **187**:6182–6199.e29.

Leonardo-Sousa, C., Barriga, R., Florindo, H. F., Acúrcio, R. C. & Guedes, R. C. (2025) Structural insights and clinical advances in small-molecule inhibitors targeting TGF-β receptor I. *Mol Ther Oncol* **33**:200945.

Li, W., Wei, Z., Liu, Y., Li, H., Ren, R. & Tang, Y. (2010) Increased 18F-FDG uptake and expression of Glut1 in the EMT transformed breast cancer cells induced by TGF-β. *Neoplasma* **57**:234–240.

Li, X., Wang, Z., Gao, B., Dai, K., Wu, J., Shen, K., …, & Chen, G. (2024) Unveiling the impact of SUMOylation at K298 site of heat shock factor 1 on glioblastoma malignant progression. *Neoplasia* **57**:101055.

Lichtman, M. K., Otero-Vinas, M. & Falanga, V. (2016) Transforming growth factor beta (TGF-β) isoforms in wound healing and fibrosis. *Wound Repair Regen* **24**:215–222.

Lin, T., Ponn, A., Hu, X., Law, B. K. & Lu, J. (2010) Requirement of the histone demethylase LSD1 in Snai1-mediated transcriptional repression during epithelial-mesenchymal transition. *Oncogene* **29**:4896–4904.

Liu, K., Tian, F., Chen, X., Liu, B., Tian, S., Hou, Y., …, & Wang, B. (2024) Stabilization of TGF-β receptor 1 by a receptor-associated adaptor dictates feedback activation of the TGF-β signaling pathway to maintain liver cancer stemness and drug resistance. *Adv Sci* 2402327.

Liu, M., Quek, L.-E., Sultani, G. & Turner, N. (2016) Epithelial-mesenchymal transition induction is associated with augmented glucose uptake and lactate production in pancreatic ductal adenocarcinoma. *Cancer Metab* **4**:19.

Lodyga, M. & Hinz, B. (2020) TGF-β1 – A truly transforming growth factor in fibrosis and immunity. *Semin Cell Dev Biol* **101**:123–139.

Mahat, D. B., Kwak, H., Booth, G. T., Jonkers, I. H., Danko, C. G., Patel, R. K., …, & Lis, J. T. (2016) Base-pair-resolution genome-wide mapping of active RNA polymerases using precision nuclear run-on (PRO-seq). *Nat Protoc* **11**:1455–1476.

Marconi, G. D., Fonticoli, L., Rajan, T. S., Pierdomenico, S. D., Trubiani, O., Pizzicannella, J. & Diomede, F. (2021) Epithelial-mesenchymal transition (EMT): the type-2 EMT in wound healing, tissue regeneration and organ fibrosis. *Cells* **10**:1587.

Massagué, J. (1998) TGF-β signal transduction. *Annu Rev Biochem* **67**:753–791.

Massagué, J. (2008) TGFβ in cancer. *Cell* **134**:215–230.

Massagué, J. & Sheppard, D. (2023) TGF-β signaling in health and disease. *Cell* **186**:4007–4037.

Mathew, A., Mathur, S. K., Jolly, C., Fox, S. G., Kim, S. & Morimoto, R. I. (2001) Stress-Specific Activation and Repression of Heat Shock Factors 1 and 2. *Mol Cell Biol* **21**:7163–7171.

Mathew, A., Mathur, S. K. & Morimoto, R. I. (1998) Heat shock response and protein degradation: regulation of HSF2 by the ubiquitin-proteasome pathway. *Mol Cell Biol* **18**:5091–5098.

Mendillo, M. L., Santagata, S., Koeva, M., Bell, G. W., Hu, R., Tamimi, R. M., …, & Lindquist, S. (2012) HSF1 Drives a Transcriptional Program Distinct from Heat Shock to Support Highly Malignant Human Cancers. *Cell* **150**:549–562.

Meng, X., Nikolic-Paterson, D. J. & Lan, H. Y. (2016) TGF-β: the master regulator of fibrosis. *Nat Rev Nephrol* **12**:325–338.

Min, J.-N., Han, M.-Y., Lee, S.-S., Kim, K.-J. & Park, Y.-M. (2000) Regulation of rat heat shock factor 2 expression during the early organogenic phase of embryogenesis. *Biochim Biophys Acta BBA - Gene Struct Expr* **1494**:256–262.

Mirzaei, S., Saghari, S., Bassiri, F., Raesi, R., Zarrabi, A., Hushmandi, K., …, & Tergaonkar, V. (2022) NF-κB as a regulator of cancer metastasis and therapy response: a focus on epithelial–mesenchymal transition. *J Cell Physiol* **237**:2770–2795.

Mivechi, N. F., Ouyang, H. & Hahn, G. M. (1992) Lower heat shock factor activation and binding and faster rate of HSP-70A messenger RNA turnover in heat sensitive human leukemias. *Cancer Res* **52**:6815–6822.

Morimoto, R. I. (2011) The heat shock response: systems biology of proteotoxic stress in aging and disease. *Cold Spring Harb Symp Quant Biol* **76**:91–99.

Moustakas, A. & Heldin, C.-H. (2012) Induction of epithelial–mesenchymal transition by transforming growth factor β. *Semin Cancer Biol* **22**:446–454.

Müller, G. A. & Engeland, K. (2021) DNA affinity purification: a pulldown assay for identifying and analyzing proteins binding to nucleic acids. In: Manfredi, J. J. (ed.), *Cell cycle checkpoints,* pp. 81-90. Springer US, New York, NY.

National Cancer Institute (2025) Cancer stat facts: female breast cancer. https://seer.cancer.gov/statfacts/html/breast.html (Accessed 29.7.2025)

Neef, D. W., Jaeger, A. M., Gomez-Pastor, R., Willmund, F., Frydman, J. & Thiele, D. J. (2014) A direct regulatory interaction between chaperonin TRiC and stress-responsive transcription factor HSF1. *Cell Rep* **9**:955–966.

Nieto, M. A., Huang, R. Y.-J., Jackson, R. A. & Thiery, J. P. (2016) EMT: 2016. *Cell* **166**:21–45.

Nykänen, P., Alastalo, T.-P., Ahlskog, J., Horelli-Kuitunen, N., Pirkkala, L. & Sistonen, L. (2001) Genomic organization and promoter analysis of the human heat shock factor 2 gene. *Cell Stress Chaperones* **6**:377–385.

Oft, M., Peli, J., Rudaz, C., Schwarz, H., Beug, H. & Reichmann, E. (1996) TGF-beta 1 and Ha-Ras collaborate in modulating the phenotypic plasticity and invasiveness of epithelial tumor cells. *GENES Dev* **10**:2462–2477.

Park, S.-M., Kim, S.-A. & Ahn, S.-G. (2015) HSF2 autoregulates its own transcription. *Int J Mol Med* **36**:1173–1179.

Peinado, H., Olmeda, D. & Cano, A. (2007) Snail, Zeb and bHLH factors in tumour progression: an alliance against the epithelial phenotype? *Nat Rev Cancer* **7**:415–428.

Pérez-González, A., Bévant, K. & Blanpain, C. (2023) Cancer cell plasticity during tumor progression, metastasis and response to therapy. *Nat Cancer* **4**:1063–1082.

Pessa, J. C., Joutsen, J. & Sistonen, L. (2024) Transcriptional reprogramming at the intersection of the heat shock response and proteostasis. *Mol Cell* **84**:80–93.

Pessa, J. C., Paavolainen, O., Hästbacka, H. S. E., Puustinen, M. C., Da Silva, A. J., Pihlström, S., …, & Sistonen, L. (2025) HSF2 drives breast cancer progression by acting as a stage-specific switch between proliferation and invasion. *Sci Adv* **11**:eady1289.

Peteranderl, R., Rabenstein, M., Shin, Y.-K., Liu, C. W., Wemmer, D. E., King, D. S. & Nelson, H. C. M. (1999) Biochemical and Biophysical Characterization of the Trimerization Domain from the Heat Shock Transcription Factor. *Biochemistry* **38**:3559–3569.

Potts, J. D. & Runyan, R. B. (1989) Epithelial-mesenchymal cell transformation in the embryonic heart can be mediated, in part, by transforming growth factor β. *Dev Biol* **134**:392–401.

Puisieux, A., Brabletz, T. & Caramel, J. (2014) Oncogenic roles of EMT-inducing transcription factors. *Nat Cell Biol* **16**:488–494.

Purwana, I., Liu, J. J., Portha, B. & Buteau, J. (2017) HSF1 acetylation decreases its transcriptional activity and enhances glucolipotoxicity-induced apoptosis in rat and human beta cells. *Diabetologia* **60**:1432–1441.

Rabindran, S. K., Haroun, R. I., Clos, J., Wisniewski, J. & Wu, C. (1993) Regulation of heat shock factor trimer formation: role of a conserved leucine zipper. *Science* **259**:230–234.

Rallu, M., Loones, Mt., Lallemand, Y., Morimoto, R., Morange, M. & Mezger, V. (1997) Function and regulation of heat shock factor 2 during mouse embryogenesis. *Proc Natl Acad Sci* **94**:2392–2397.

Raychaudhuri, S., Loew, C., Körner, R., Pinkert, S., Theis, M., Hayer-Hartl, M., …, & Hartl, F. U. (2014) Interplay of acetyltransferase EP300 and the proteasome system in regulating heat shock transcription factor 1. *Cell* **156**:975–985.

Ren, Q., Li, L., Liu, L., Li, J., Shi, C., Sun, Y., …, & Xiang, S. (2025) The molecular mechanism of temperature-dependent phase separation of heat shock factor 1. *Nat Chem Biol* **21**:831–842.

Ritossa, F. (1962) A new puffing pattern induced by temperature shock and DNP in drosophila. *Experientia* **18**:571–573.

Romano, L. A. & Runyan, R. B. (2000) Slug is an Essential Target of TGFβ2 Signaling in the Developing Chicken Heart. *Dev Biol* **223**:91–102.

Ruoslahti, E. (1981) Fibronectin. *J Oral Pathol Med* **10**:3–13.

Sandqvist, A., Björk, J. K., Åkerfelt, M., Chitikova, Z., Grichine, A., Vourc'h, C., …, & Sistonen, L. (2009) Heterotrimerization of Heat-Shock Factors 1 and 2 Provides a Transcriptional Switch in Response to Distinct Stimuli. *Mol Biol Cell* **20**:1340–1347.

Sarge, K. D., Zimarino, V., Holm, K., Wu, C. & Morimoto, R. I. (1991) Cloning and characterization of two mouse heat shock factors with distinct inducible and constitutive DNA-binding ability. *Genes Dev* **5**:1902–1911.

Sarge, K. D., Park-Sarge, O.-K., Kirby, J. D., Mayo, K. E. & Morimoto, R. I. (1994) Expression of heat shock factor 2 in mouse testis: potential role as a regulator of heat-shock protein gene expression during spermatogenesis. *Biol Reprod* **50**:1334–1343.

Satelli, A. & Li, S. (2011) Vimentin in cancer and its potential as a molecular target for cancer therapy. *Cell Mol Life Sci* **68**:3033–3046.

Sawicki, S. G. & Godman, G. C. (1971) On the differential cytotoxicity of actinomycin D. *J Cell Biol* **50**:746–761.

Scheel, C., Eaton, E. N., Li, S. H.-J., Chaffer, C. L., Reinhardt, F., Kah, K.-J., …, & Weinberg, R. A. (2011) Paracrine and autocrine signals induce and maintain mesenchymal and stem cell states in the breast. *Cell* **145**:926–940.

Scherz-Shouval, R., Santagata, S., Mendillo, M. L., Sholl, L. M., Ben-Aharon, I., Beck, A. H., …, & Lindquist, S. (2014) The reprogramming of tumor stroma by HSF1 is a potent enabler of malignancy. *Cell* **158**:564–578.

Schuetz, T. J., Gallo, G. J., Sheldon, L., Tempst, P. & Kingston, R. E. (1991) Isolation of a cDNA for HSF2: evidence for two heat shock factor genes in humans. *Proc Natl Acad Sci* **88**:6911–6915.

Sechopoulos, I., Teuwen, J. & Mann, R. (2021) Artificial intelligence for breast cancer detection in mammography and digital breast tomosynthesis: state of the art. *Semin Cancer Biol* **72**:214–225.

Shen, W., Tao, G., Zhang, Y., Cai, B., Sun, J. & Tian, Z. (2017) TGF-β in pancreatic cancer initiation and progression: two sides of the same coin. *Cell Biosci* **7**:39.

Shi, X., Yang, J., Deng, S., Xu, H., Wu, D., Zeng, Q., …, & Zhou, H. (2022) TGF-β signaling in the tumor metabolic microenvironment and targeted therapies. *J Hematol Oncol* **15**:135.

Shi, Y., Kroeger, P. E. & Morimoto, R. I. (1995) The carboxyl-terminal transactivation domain of heat shock factor 1 is negatively regulated and stress responsive. *Mol Cell Biol* **15**:4309–4318.

Silver, J. T. & Noble, E. G. (2012) Regulation of survival gene hsp70. *Cell Stress Chaperones* **17**:1–9.

Sisto, M. & Lisi, S. (2024) Epigenetic regulation of EMP/EMT-dependent fibrosis. *Int J Mol Sci* **25**:2775.

Sistonen, L., Sarge, K. D. & Morimoto, R. I. (1994) Human heat shock factors 1 and 2 are differentially activated and can synergistically induce hsp70 gene transcription. *Mol Cell Biol* **14**:2087–2099.

Sivéry, A., Courtade, E. & Thommen, Q. (2016) A minimal titration model of the mammalian dynamical heat shock response. *Phys Biol* **13**:066008.

Skrypek, N., Goossens, S., De Smedt, E., Vandamme, N. & Berx, G. (2017) Epithelial-to-mesenchymal transition: epigenetic reprogramming driving cellular plasticity. *Trends Genet* **33**:943–959.

Smith, R. S., Takagishi, S. R., Amici, D. R., Metz, K., Gayatri, S., Alasady, M. J., …, & Mendillo, M. L. (2022) HSF2 cooperates with HSF1 to drive a transcriptional program critical for the malignant state. *Sci Adv* **8**:eabj6526.

Sun, X., Malandraki-Miller, S., Kennedy, T., Bassat, E., Klaourakis, K., Zhao, J., …, & Riley, P. R. (2021) The extracellular matrix protein agrin is essential for epicardial epithelial-to-mesenchymal transition during heart development. *Development* **148**:dev197525.

Tan, T., Shi, P., Abbas, M. N., Wang, Y., Xu, J., Chen, Y. & Cui, H. (2022) Epigenetic modification regulates tumor progression and metastasis through EMT (Review). *Int J Oncol* **60**:70.

Tateishi, Y., Ariyoshi, M., Igarashi, R., Hara, H., Mizuguchi, K., Seto, A., …, & Shirakawa, M. (2009) Molecular Basis for SUMOylation-dependent Regulation of DNA Binding Activity of Heat Shock Factor 2*. *J Biol Chem* **284**:2435–2447.

Thermo Fisher Scientific (2009) *Acetone precipitation of proteins* (Application Note No. TR0049). https://assets.thermofisher.com/TFS-Assets/LSG/ApplicationNotes/TR0049Acetone-precipitation.pdf (Accessed 29.7.2025).

Thiery, J. P. & Sleeman, J. P. (2006) Complex networks orchestrate epithelial–mesenchymal transitions. *Nat Rev Mol Cell Biol* **7**:131–142.

Thuault, S., Tan, E.-J., Peinado, H., Cano, A., Heldin, C.-H. & Moustakas, A. (2008) HMGA2 and Smads co-regulate SNAIL1 expression during induction of epithelial-to-mesenchymal transition *. *J Biol Chem* **283**:33437–33446.

Thuault, S., Valcourt, U., Petersen, M., Manfioletti, G., Heldin, C.-H. & Moustakas, A. (2006) Transforming growth factor-β employs HMGA2 to elicit epithelial–mesenchymal transition. *J Cell Biol* **174**:175–183.

Trelstad, R. L., Hayashi, A., Hayashi, K. & Donahoe, P. K. (1982) The epithelial-mesenchymal interface of the male rat Mullerian duct: loss of basement membrane integrity and ductal regression. *Dev Biol* **92**:27–40.

Urban, L., Čoma, M., Lacina, L., Szabo, P., Sabová, J., Urban, T., …, & Gál, P. (2023) Heterogeneous response to TGF-β1/3 isoforms in fibroblasts of different origins: implications for wound healing and tumorigenesis. *Histochem Cell Biol* **160**:541–554.

Vincent, T., Neve, E. P. A., Johnson, J. R., Kukalev, A., Rojo, F., Albanell, J., …, & Fuxe, J. (2009) A SNAIL1–SMAD3/4 transcriptional repressor complex promotes TGF-β mediated epithelial–mesenchymal transition. *Nat Cell Biol* **11**:943–950.

Wang, G., Zhang, J., Moskophidis, D. & Mivechi, N. F. (2003) Targeted disruption of the heat shock transcription factor (*hsf*)-2 gene results in increased embryonic lethality, neuronal defects, and reduced spermatogenesis. *Genesis* **36**:48–61.

Wang, Y., Shi, J., Chai, K., Ying, X. & Zhou, B. P. (2013) The role of snail in EMT and tumorigenesis. *Curr Cancer Drug Targets* **13**:963–972.

Weinberg, R. A. (2023) *The biology of cancer*. 3rd edition, international student edition. W. W. Norton & Company, New York, NY and London.

Wendt, M. K., Tian, M. & Schiemann, W. P. (2012) Deconstructing the mechanisms and consequences of TGF-β-induced EMT during cancer progression. *Cell Tissue Res* **347**:85–101.

Westerheide, S. D., Anckar, J., Stevens, S. M., Sistonen, L. & Morimoto, R. I. (2009) Stress-inducible regulation of heat shock factor 1 by the deacetylase SIRT1. *Science* **323**:1063–1066.

Xiao, X. (1999) HSF1 is required for extra-embryonic development, postnatal growth and protection during inflammatory responses in mice. *EMBO J* **18**:5943–5952.

Xie, L., Law, B. K., Chytil, A. M., Brown, K. A., Aakre, M. E. & Moses, H. L. (2004) Activation of the Erk pathway is required for TGF-β1-induced EMT in vitro. *Neoplasia* **6**:603–610.

Xu, D., Zalmas, L. P. & La Thangue, N. B. (2008) A transcription cofactor required for the heat-shock response. *EMBO Rep* **9**:662–669.

Xue, W., Yang, L., Chen, C., Ashrafizadeh, M., Tian, Y. & Sun, R. (2024) Wnt/β-catenin-driven EMT regulation in human cancers. *Cell Mol Life Sci* **81**:79.

Yamamoto, N., Takemori, Y., Sakurai, M., Sugiyama, K. & Sakurai, H. (2009) Differential recognition of heat shock elements by members of the heat shock transcription factor family. *FEBS J* **276**:1962–1974.

Yamazaki, S., Iwama, A., Takayanagi, S., Eto, K., Ema, H. & Nakauchi, H. (2009) TGF-β as a candidate bone marrow niche signal to induce hematopoietic stem cell hibernation. *Blood* **113**:1250–1256.

Yang, H.-L., Chang, C.-W., Vadivalagan, C., Pandey, S., Chen, S.-J., Lee, C.-C., …, & Hseu, Y.-C. (2024) Coenzyme Q0 inhibited the NLRP3 inflammasome, metastasis/EMT, and Warburg effect by suppressing hypoxia-induced HIF-1α expression in HNSCC cells. *Int J Biol Sci* **20**:2790–2813.

Yang, J., Antin, P., Berx, G., Blanpain, C., Brabletz, T., Bronner, M., …, & Sheng, G. (2020) Guidelines and definitions for research on epithelial–mesenchymal transition. *Nat Rev Mol Cell Biol* **21**:341–352.

Yoshimura, S., Shimada, R., Kikuchi, K., Kawagoe, S., Abe, H., Iisaka, S., …, & Ishiguro, K. (2024) Atypical heat shock transcription factor HSF5 is critical for male meiotic prophase under non-stress conditions. *Nat Commun* **15**:3330.

Zaravinos, A. (2015) The regulatory tole of microRNAs in EMT and cancer. *J Oncol* **2015**:865816.

Zhang, M., Zhao, A., Guo, C. & Guo, L. (2021) A combined modelling and experimental study of heat shock factor SUMOylation in response to heat shock. *J Theor Biol* **530**:110877.

Zi, Z., Feng, Z., Chapnick, D. A., Dahl, M., Deng, D., Klipp, E., …, & Liu, X. (2011) Quantitative analysis of transient and sustained transforming growth factor-β signaling dynamics. *Mol Syst Biol* **7**:492.

Åkerfelt, M., Henriksson, E., Laiho, A., Vihervaara, A., Rautoma, K., Kotaja, N. & Sistonen, L. (2008) Promoter ChIP-chip analysis in mouse testis reveals Y chromosome occupancy by HSF2. *Proc Natl Acad Sci* **105**:11224–11229.

Östling, P., Björk, J. K., Roos-Mattjus, P., Mezger, V. & Sistonen, L. (2007) Heat shock factor 2 (HSF2) Contributes to inducible expression of hsp genes through interplay with HSF1 *. *J Biol Chem* **282**:7077–7086.

Appendix

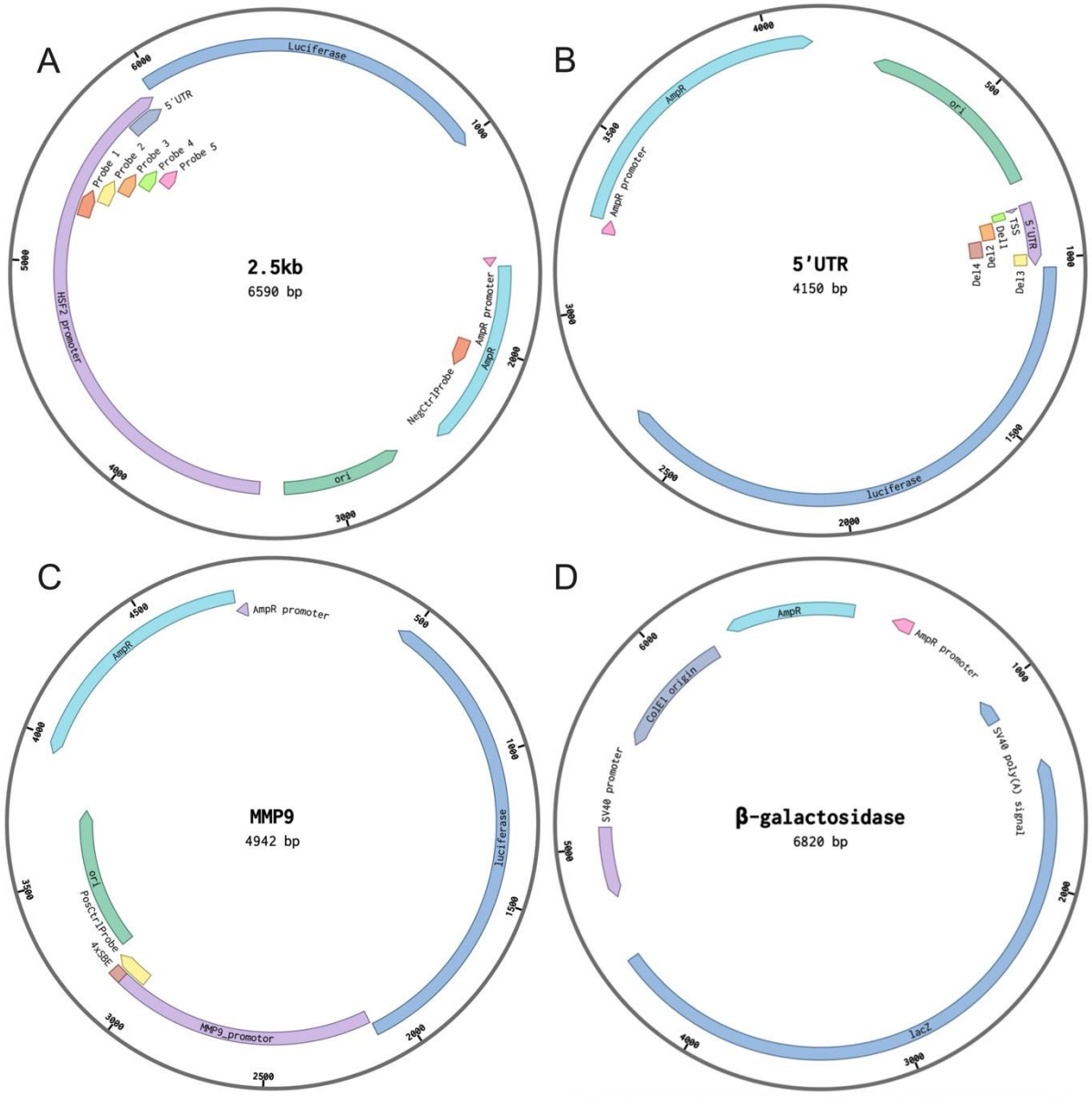

Figure S1. Annotated plasmid maps of constructs used in this thesis, designed in and acquired from Benchling. (A) *HSF2*-promoter plasmid (2.5-kb): Contains the luciferase (*luc*) gene encoding firefly luciferase, with annotated regions indicating amplification sites for DNA probes 1–5 and the negative control probe (NegCtrlProbe). (B) 5'UTR plasmid: Contains the *luc* gene with annotated deletions in the 5'untranslated region (5'UTR), corresponding to sequences omitted during generation of deletion variants (ΔDel1–4). (C**)** MMP9 promoter plasmid: Contains the *luc* gene driven by the MMP9 promoter with four Smad binding elements (SBEs); the amplified region for the positive control DNA probe is indicated (PosCtrlProbe). (D) Commercial β-galactosidase plasmid: Contains the *lacZ* gene encoding β-galactosidase, under the control of a constitutive simian virus 40 promoter. Additionally, all plasmids contain the ampicillin resistance gene (*AmpR*) and its promoter.

Table S1. Nuclear extraction buffer compositions tested during protocol optimization. Each buffer was evaluated for extract yield and fraction specificity. All buffers were supplemented with 0.5 mM DTT and protease inhibitors. EDTA, ethylenediaminetetraacetic acid; HEPES, 4-(2-hydroxyethyl)-1-piperazineethanesulfonic acid; Tris, tris(hydroxymethyl)aminomethane.

Composition	*Reference*	*Reasons not selected*
10 mM HEPES-KOH, 1.5 mM $MgCl_2$, 10 mM KCl, pH 7.9	(Müller and Engeland 2021)	Incomplete membrane disruption, poor fraction specificity
10 mM Tris-HCl pH 7.9, 1.5 mM $MgCl_2$, 10 mM KCl, 300 mM sucrose	Modified from (Müller and Engeland 2021)	Incomplete membrane disruption, poor fraction specificity
10 mM Tris-HCl pH 7.9, 300 mM sucrose, 3 mM $CaCl_2$, 2 mM $MgCl_2$, 0.1% Triton X-100	Modified from (Mahat et al. 2016)	Cytoplasmic markers found in nuclear fraction
10 mM Tris-HCl pH 7.9, 300 mM sucrose, 3 mM $CaCl_2$, 2 mM $MgCl_2$, 0.1% NP-40	Modified from (Mahat et al. 2016)	Cytoplasmic markers found in nuclear fraction
10 mM Tris-HCl pH 7.9, 3 mM $CaCl_2$, 2 mM $MgCl_2$, 0.1% Triton X-100	Modified from (Mahat et al. 2016)	-

Table S2. Nuclear lysis buffer compositions tested during protocol optimization. Each buffer was evaluated for fraction specificity. All buffers were supplemented with 0.5 mM DTT and protease inhibitors.

Composition	*Reference*	*Reasons not selected*
20 mM HEPES-KOH, 1.5 mM MgCl2, 0.2 mM EDTA, pH 7.9, additionally supplemented with 450 mM NaCl	(Müller and Engeland 2021)	Incomplete nuclear membrane disruption
20 mM Tris-HCl pH 7.9; 1.5 mM $MgCl_2$; 0.2 mM EDTA, additionally supplemented with 450 mM NaCl and 25% glycerol		Incomplete nuclear membrane disruption
RIPA buffer	In-house protocol	-

Script S1. Analysis of raw luminescence data. This script analyzes raw luciferase activity (β-gal–normalized) relative to control, by performing one-tailed paired t-tests, and adjusting p-values using the Benjamini-Hochberg FDR method.

```
library(dplyr)
library(tidyr)
# HSF2 constructs are tested for repression (mean < 1), whereas MMP9 is tested for
 activation (mean > 1).
get_alt_direction <- function(construct) {
  if (construct == "MMP9") "greater" else "less"
}
# Significance annotation
get_signif <- function(p) {
```

```
  ifelse(p < 0.0001, "****",
  ifelse(p < 0.001,  "***",
  ifelse(p < 0.01,   "**",
  ifelse(p < 0.05,   "*", "ns"))))
}
# Raw β-gal normalized luciferase values
luc_raw <- tribble(
  ~Construct, ~C1, ~C2, ~C3, ~C4, ~C5, ~C6,
              ~T1, ~T2, ~T3, ~T4, ~T5, ~T6,
  "2.5kb",    1894222.85, 3128376.07, 2441950, NA, NA, NA,
              1087213.94, 870931.17, 662295.96, NA, NA, NA,
  "2kbΔ0.5kb",100533.54, 61361.55, 84379.59, NA, NA, NA,
              51184.8, 48641.31, 49956.83, NA, NA, NA,
  "1kb",      2670219.44, 3088483.17, 4540038.96, NA, NA, NA,
              1684710.32, 1210043.38, 1054739.84, NA, NA, NA,
  "1kbΔ5'UTR",201704.33, 59494.02, 121080.06, 106590.91, 87451.35, 103872.81,
              71665.04, 21669.9, 39258.1, 37676.39, 29328.24, 31448.89,
  "0.5kb",    2272501.11, 1723586.43, 2585725.13, NA, NA, NA,
              366044.51, 392389.63, 362062.09, NA, NA, NA,
  "5'UTR",    236293.71, 141138.01, 340702.23, 253330.75, 235876.85, 225185.76,
              107329.84, 62021.66, 153328.03, 205911.65, 184079.12, 103928.86,
  "ΔDel1",    599322.58, 145057.47, 501150.14, NA, NA, NA,
              236151.52, 110155.64, 426447.67, NA, NA, NA,
  "ΔDel2",    48292.27, 39837.73, 109572.79, NA, NA, NA,
              27207.25, 16625.34, 52314.34, NA, NA, NA,
  "ΔDel3",    78434.07, 69982.61, 133211.76, NA, NA, NA,
              28307.51, 28032.39, 74275.71, NA, NA, NA,
  "ΔDel4",    13191.69, 11846.84, 33621.55, NA, NA, NA,
              8424.4, 7182.44, 23836.36, NA, NA, NA,
  "MMP9",     73608.09, 74578.66, 96151.04, 59143.33, 79378.28, 144885.79,
              212478.34, 146303.41, 189801.02, 301876.61, 190713.99, 450671.4
)
# Paired tests
paired_results <- luc_raw%>%
  rowwise()%>%
  do({
    construct <- .$Construct
    # Extract vectors
    control <- as.numeric(c(.$C1, .$C2, .$C3, .$C4, .$C5, .$C6))
```

```
    treated <- as.numeric(c(.$T1, .$T2, .$T3, .$T4, .$T5, .$T6))
    # Keep only paired values
    df <- data.frame(C = control, T = treated)
    df <- df[!is.na(df$C) & !is.na(df$T), ]
    # Skip if <2 pairs
    if (nrow(df) < 2) {
      return(tibble(Construct = construct, n = nrow(df),
                    mean_Control = NA_real_, mean_TGFb = NA_real_,
                    FC = NA_real_, p_value = NA_real_))
    }
    alt <- get_alt_direction(construct)
    tt <- t.test(df$T, df$C, paired = TRUE, alternative = alt)
    tibble(
      Construct    = construct,
      n            = nrow(df),
      mean_Control = mean(df$C),
      mean_TGFb    = mean(df$T),
      FC           = mean(df$T) / mean(df$C),
      p_value      = tt$p.value
    )
  })%>%
  ungroup()
# Add corrections and significance annotations
paired_results <- paired_results%>%
  mutate(
    p_adj_BH   = p.adjust(p_value, method = "BH"),
    Signif     = get_signif(p_value),
    Signif_BH  = get_signif(p_adj_BH)
  )
print(paired_results)
```

Script S2. Analysis of fold-change data. This script analyzes fold changes relative to control, performs one-sample one-tailed t-tests, and adjusts p-values using the Benjamini-Hochberg FDR method.

```
library(dplyr)
library(purrr)
# TGF-β/control ratios per construct. Each row is a construct; each column is a
 biological replicate (NA = no measurement).
luc_fc <- data.frame(
  `2.5kb`        = c(0.57, 0.28, 0.27, NA, NA, NA),
```

```
  `2kbΔ0.5kb`     = c(0.51, 0.79, 0.59, NA, NA, NA),
  `1kb`           = c(0.63, 0.39, 0.23, NA, NA, NA),
  `1kbΔ5'UTR`     = c(0.36, 0.36, 0.32, 0.35, 0.34, 0.30),
  `0.5kb`         = c(0.16, 0.23, 0.14, NA, NA, NA),
  `5'UTR`         = c(0.45, 0.44, 0.45, 0.81, 0.78, 0.46),
  `ΔDel1`         = c(0.39, 0.76, 0.85, NA, NA, NA),
  `ΔDel2`         = c(0.56, 0.42, 0.48, NA, NA, NA),
  `ΔDel3`         = c(0.36, 0.40, 0.56, NA, NA, NA),
  `ΔDel4`         = c(0.64, 0.61, 0.71, NA, NA, NA),
  `MMP9`          = c(2.89, 1.96, 1.97, 5.10, 2.40, 1.24)
)
# One-tailed direction per construct, HSF2 constructs are tested for repression
 (mean < 1), whereas MMP9 is tested for activation (mean > 1).
get_alt_direction <- function(construct) {
  if (construct == "MMP9") {
    "greater"    # test for activation (TGF-β > 1)
  } else {
    "less"       # test for repression (TGF-β < 1)
  }
}
# Significance annotation
get_signif <- function(p) {
  ifelse(p < 0.0001, "****",
  ifelse(p < 0.001,  "***",
  ifelse(p < 0.01,   "**",
  ifelse(p < 0.05,   "*", "ns"))))
}
# One-sample, one-tailed t-tests vs μ = 1 for each construct (repression for HSF2
 constructs, activation for MMP9).
fc_results <- map_dfr(
  names(luc_fc),
  ~{
    construct <- .x
    x <- luc_fc[[construct]]
    x <- x[!is.na(x)]
    alt <- get_alt_direction(construct)
    tt <- t.test(x,
                 mu          = 1,
                 alternative = alt,
                 conf.level  = 0.95)
```

```
    tibble(
      Construct   = construct,
      n           = length(x),
      Mean        = mean(x),
      SD          = sd(x),
      t_stat      = unname(tt$statistic),
      alternative = alt,
      p_value     = tt$p.value
    )
  }
)
# Add corrections and significance annotation
fc_results <- fc_results%>%
  mutate(
    p_adj_BH   = p.adjust(p_value, method = "BH"),
    Signif     = get_signif(p_value),
    Signif_BH  = get_signif(p_adj_BH)
  )
print(fc_results)
```